

Wing. L. M. A. L.

Copy  
~~876~~

TECHNICAL MEMORANDUMS  
NATIONAL ADVISORY COMMITTEE FOR AERONAUTICS

No. 876

INVESTIGATIONS ON THE DOWNWASH BEHIND A  
TAPERED WING WITH FUSELAGE AND PROPELLER

By H. Muttrey

Luftfahrtforschung  
Vol. 15, No. 3, March 20, 1938  
Verlag von R. Oldenbourg, München und Berlin

Washington  
September 1938

12.2.7  
1.8.1.1.1  
17.1.1.1  
1.5.4



3 1176 01440 3563

NATIONAL ADVISORY COMMITTEE FOR AERONAUTICS

TECHNICAL MEMORANDUM NO. 876

INVESTIGATIONS ON THE DOWNWASH BEHIND A  
TAPERED WING WITH FUSELAGE AND PROPELLER\*

By H. Muttray

SUMMARY

The new downwash measurements behind a tapered wing with parallel center section described in the present report can be brought into good agreement with theoretical calculations if made on the basis of not-rolled-up vortex sheet and allowance is made for the lowering of the sheet. The test values are about  $1^\circ$  higher than the "upper limit" established for it, as against approximately  $0.5^\circ$  in the earlier tests behind a rectangular and elliptical wing. The measurements on lateral axes, especially if lying below the wing on a level with the vortex train, disclosed in accord with the lift distribution, a marked change in angle over the span of the tail in contrast to the rectangular and elliptical wing.

The downwash measurements on the low-wing model without propeller running indicate only a minor effect of fuselage on the downwash with "ideal" fuselage in comparison to "wing alone." But for "angular" fuselage, the effect, even though it also extends only over a comparatively narrow width, is quite pronounced, that is, in the sense of an improvement in static longitudinal stability.

The downwash measurements on low-wing models with propeller running disclose a very strongly expressed slipstream twist in vicinity of the tail despite the rectifying effect of the wing. There are other disturbed downwash zones to both sides of this twist region. The prefix of the disturbances - of different extent to left and right - is in these zones the opposite of that of the slipstream twist.

---

\*"Untersuchungen über den Abwind hinter einem Trapezflügel mit Rumpf und Schraube." Luftfahrtforschung, vol. 15, no. 3, March 20, 1938, pp. 101-122.

The downwash distribution over a lateral axis approximately in tail vicinity - the same holds for the velocity distribution in the slipstream also - becomes very unsymmetrical with increasing angle of attack as a result of the yaw of the propeller.

The magnitude of supplementary angle of downwash averaged over a span of  $\pm 0.3$  of that of the wing, with propeller running (compared to model without it) amounts at the most (at maximum angle of attack and maximum propeller loading) to no more than about  $1.5^\circ$  at wing level. For fixed angle of attack the angle of additional downwash grows linearly with the propeller loading. It is greater on the low-wing model with angular fuselage than on that with ideal fuselage. It is - like the mean angle of downwash of the low-wing models without propeller - materially influenced by the height level of the tail.

In a stability comparison of both models at equal full throttle polar, the model with angular fuselage is superior, the consideration concerning an airplane of conventional design, that is, in our case, with body-fixed horizontal tail surface. Again this is primarily associated with the dissimilar course of the mean angle of downwash on the height level of the tail.

With assumedly wind-fixed horizontal tail surface, i.e., constant level  $\epsilon_h$  at increasing  $\alpha$ , the stability increases enormously. A further increase may be looked for if, with changing  $\alpha$ , not only the tail but the "fuselage with slipstream" as well remain wind-fixed (say by changing the wing incidence relative to the fuselage).

#### A. INTRODUCTION

Earlier studies on the downwash behind wings of rectangular and elliptic plan form (reference 1) related to the question of dependence of downwash behind a wing on the data of the wing alone, whereby temporarily, to be sure, merely different plan forms were included in the investigation. It was found that the downwash coefficients differed considerably in correspondence with the different lift distributions of the explored wings. The present investigation was to treat other essential factors governing the magnitude of the downwash. They are particularly: the fuselage and the propeller slipstream. As the present inves-

tigation was to follow as closely as possible the previous studies, a wing of different plan form without twist was chosen purposely.

## B. MODEL DESCRIPTION AND POLARS OF THE MODELS WITHOUT PROPELLER RUNNING

The three-piece tapered wing with rectangular center section and rounded tips is illustrated in figure 1. The employed Göttingen airfoil section No. 747 is a pure

Joukowski airfoil with  $\frac{d}{l} = 0.10$  and  $\frac{f}{l} = 0.125$ . The taper ratio is  $\frac{t_a}{t_i} = 0.333$ , the ratio of center-section span to total wing span is  $\frac{b_1}{b} = 0.17$ . The choice of these particular ratios was prompted by the desire for an approximately elliptic lift distribution (reference 2). The span of the model was 1.0 m.

The described wing was successively fitted with different bodies in low-wing arrangement, as indicated in figure 1. The "angular body" resembles in its design that commonly used in airplane construction, while the "ideal body" evinces a progressive transition from maximum body height to profile chord of the wing. Body and fillets were in one piece and on the low wing with ideal body took the place of the rectangular center section.

The axis of the angular body which coincides with the propeller axis has a  $3^\circ$  incidence relative to the profile chord of the wing. The choice for this rather large angle was prompted by the desire to bring out the flow around the wing and thus emphasize the downwash. The shape of the so-called "ideal body" on the other hand was to avoid such flows as much as possible. The lateral contour of the ideal body resulted, according to previously applied method (reference 3), from the streamline pattern of "wing alone," i.e., it was adapted to the flow around the wing prescribed for a certain angle of attack of the wing, which amounted to  $3^\circ$ , corresponding to a value of  $c_a = 0.9$ . For "wing alone" and for "low wing with ideal body" this angle of attack accordingly had to give approximately the same lift  $c_a$ . And the polars (fig. 2) confirm this expectation quite

closely. But on the "low wing with angular body" by reason of form and incidence of the body relative to the wing an equal  $c_a$  value of "wing alone" and "wing with body" was not to occur until at a higher angle of attack. This angle lies at around  $\alpha = 9^\circ$  according to the polars of figure 2.

The comparatively large angle of setting of the "angular body" necessitated on the low-wing model a small cut-away at the trailing edge which, however, could have had no special effect on the polar and the downwash conditions. Inversely the wing area of the "low-wing model with ideal body" is increased through the wing roots. The differences in the  $c_{a_{max}}$  values of the polars are probably connected with it.

The propeller is mounted approximately at  $1/4$  of half the propeller diameter over the wing chord and at about  $3/4$  of the diameter ahead of the wing center. The inclination of the propeller axis to the profile chord on both low-wing models is  $3^\circ$  in the sense of an air flow of the pressure side of the profile through the slipstream. The propeller diameter is equal to  $0.2 b$  ( $b = \text{span of model}$ ), the ratio of swept-disk area to wing area is  $1:4.5$ . The counter-clockwise rotating propeller is of the type  $S_1 F_2 A_1 P_1$  from N.A.C.A. Technical Report No. 141 (reference 4). The pitch is  $H = 0.7 D$  (fig. 3). Neither the performance coefficients nor the slipstream deflection or twist were measured on the propeller running by itself. The characteristic curves (fig. 4) of the propeller running alone were taken from N.A.C.A. Report No. 141 (reference 4). The dashed curve indicates the  $k_p$  values based respectively on the polar of the "low-wing" model with ideal fuselage and the  $c_w$  values of figure 7.

The forces with propeller running were measured at seven angles of attack. Lift, drag, and pitching moment were measured at increasing r.p.m., including the r.p.m. range between zero thrust and stopped propeller (once vertical, once horizontal).

### C. TEST PROCEDURE AND EVALUATION

In contrast with the earlier measurements (reference 1), which were carried out in tunnel I of 2.25 m diameter at the AVA Göttingen, the present measurements were made in "small tunnel" (tunnel II) of the AVA. Having enlarged

the open jet with an elliptic nozzle of 1.5 m width and 1.05 m depth it was possible to retain the same model span:  $b = 1.0$  m.

Because of the small jet section of  $1.2 \text{ m}^2$  as compared to the  $4.0 \text{ m}^2$  of tunnel I with 2.25 m diameter, the corrections, necessary for reducing the data from the "small tunnel" to infinitely great stream section were of course substantially greater. These were computed on the basis of the report by I. Lotz on the corrections of downwash in the open jet of elliptic section (reference 5), whereby the lift coefficient of the "wing alone" served as a basis for equal angle of attack of the models "wing alone," "wing with fuselage" and "wing with fuselage and propeller running".

The downwash factors are presented in a nondimensional system of coordinates, with its zero point in the aerodynamic center of the mean line of the wing. In the separate graphs of the angles of downwash for "wing alone" these angles are, as in the earlier investigations (reference 1) also given nondimensionally. It is

$l$  is distance of the test point from the bound vortex in direction of the longitudinal axis downstream

$q$ , distance of test point from the plane of symmetry of the wing in lateral axis direction (+  $q$  = starboard wing)

$h$ , distance of test point in vertical axis direction (+  $h$  = suction side, -  $h$  = pressure side)

$\epsilon_l = \frac{l}{b/2}$ ,  $\epsilon_q = \frac{q}{b/2}$ ,  $\epsilon_h = \frac{h}{b/2}$ , distance factors

$\frac{\alpha_w}{\alpha_l}$ , coefficient of downwash

The reason for plotting the angles of downwash on the low-wing models in radians was due to the fact - as the test data will prove - that in the downwash the twist of the slipstream is very pronounced, whereas there is no reason to refer the same additional downwash due to twist at variable lift and equal coefficient of advance to the variable, induced angle of attack.

The first downwash measurements behind the models without propeller running were made with small silk threads because the dual tube downwash recorder used in the earlier studies (reference 1) was not available, though it did arrive in time for the tests on models with propeller running. To afford a better comparison of the test data "with" and "without propeller running," a great portion of the downwash measurements behind the models "without propeller running" were repeated with the dual tube downwash recorder.\* At this place only a very few of the comparative curves plotted by the two methods will be shown, while for the rest the more exact results achieved with the dual tube instrument will be given.

Figure 5 illustrates - nondimensionally - for "wing alone" the results obtained on three lateral axes at distance  $\epsilon_l = 1.0$  from the wing. The agreement is, in general, good, except for the lateral axis in the pressure-side position  $\epsilon_h = -0.2$ , where greater discrepancies exist. The cause of this is that this lateral axis lies exactly at the height of the maximum downwash values, as seen from figure 6. It includes, for instance, the comparison between thread measurement and dual tube record for a vertical axis located at distance  $\epsilon_l = 1.0$  for  $\epsilon_q = 0.12$ . It is seen that the points of the thread measurements in proximity of the maximum values were figured as one-sided scattering points, resulting in the dashed curve. (The peak in the vertical-axis curves was not expected after the results of the earlier measurements on the elliptical and rectangular wing (reference 1). (Cf. fig. 15.)) The air speed for these downwash measurements was  $v = 21.0$  m/s.

## D. RESULTS

### I. FORCE MEASUREMENTS

The results of the force measurements are shown nondimensionally in figures 7 to 9 for the "low wing with ideal fuselage" and in figures 10 to 12 for "low wing with angular fuselage" plotted against the reciprocal value of the coef-

ficient of advance  $\frac{1}{\lambda} = \frac{u}{v}$ . The graphs for  $c_a$  and  $c_w$

---

\*Some special experiences gained with this instrument are to be published in "Luftfahrtforschung."

against  $\frac{1}{\lambda}$  (figs. 7, 8, 10, and 11) also contain pieces of curves extending only over a limited  $\frac{u}{v}$  range. These pieces indicate the values at which the downwash was recorded. The graphs for  $c_w$  against  $\frac{u}{v}$  (figs. 7 and 10) contain, moreover, as dashed lines the coefficients of the "reference measurements," i.e., in this case of the measurements with propeller removed. The intersection of these straight lines with the curves gives the coefficient of advance for thrust equal zero. To the left of this intersection the propeller operates as (decelerated) windmill. The maximum additional drag in this range is therefore not created with stopped propeller but at a value of  $u/v$  located much closer to the point for zero thrust, more exactly, at the point for maximum torque output. At point  $\frac{1}{\lambda} = 0$  the smaller  $c_w$  values are on the whole applicable to the propeller blades in vertical position.

The polars, figures 13 and 14, are developed from figures 7 to 12. They indicate that the lift coefficient at equal angle of attack corresponding to the low-wing arrangement increases with decreasing coefficient of advance, although this rise is not very important. As the coefficient of advance decreases, the  $c_m$  value increases again. ✓

## II. DOWNWASH MEASUREMENTS

### 1. Scope of Measurements

For "wing alone," these measurements extended over an angle-of-attack range from  $\alpha = -4^\circ$  to  $\alpha = +15^\circ$ ; for "low wing with ideal fuselage" and propeller running, they included  $\alpha = 3.15^\circ$ ,  $\alpha = 6.8^\circ$ , and  $\alpha = 10.6^\circ$ , and for "low wing with angular fuselage" over  $\alpha = -0.6^\circ$ ,  $+3.15^\circ$ ,  $6.85^\circ$ , and  $10.6^\circ$ . On the model with ideal fuselage, the measurements were made at  $\alpha = 3.15^\circ$  for five different r.p.m. - one at zero thrust and one in the windmill range of r.p.m. - and at  $\alpha = 6.85^\circ$  and  $10.6^\circ$  at one r.p.m. each for approximately horizontal flight ( $c_w = 0$ ). On the "low wing with angular fuselage" the measurements were made at every angle of attack for three r.p.m., which likewise ranged around  $c_w = 0$ .

Thus the measurement was not extended very much into the climbing range (high propeller loading). Nevertheless, it will be seen that extrapolation affords some safe predictions concerning the climbing range (figs. 48, 49, 64, and 65). For the time being the principal aim was to create a general picture of the flow phenomena around the tail with propeller running and different fuselage forms. This also explains our preference for the point-by-point measurement with the dual tube instrument which at the same time allows accurate averaging. It was also the reason for the searching velocity distribution measurement - although only on the low-wing model with angular fuselage and only at one angle of attack and one coefficient of advance in vicinity of the tail ( $\epsilon_1 = 1.0$ ).

The downwash measurements were largely effected in a transverse plane at  $\epsilon_1 = 1.0$  distance from the wing, extending over three to six lateral axes and three vertical axes. On the low-wing models they were supplemented by measurements on two horizontal axes above or below the fuselage in the plane of symmetry of the model and to the right and left of the fuselage at height  $\epsilon_h = 0$ , although the measurements did not include different r.p.m. for all axes. Individual reference measurements, moreover, must be obtained by interpolation. On the "wing alone" it further included the longitudinal axis at wing height and in the plane of symmetry.

## 2. Aspect of Downwash Curves

### a. Wing Alone

Vertical axes.- Figure 6 shows for  $\alpha = 6.8^\circ$  the nondimensional angles of downwash on a vertical axis at distance  $\epsilon_1 = 1.0$  and approximately in the plane of symmetry of the wing at  $\epsilon_q = 0.12$ . These values may be equated to those of the plane of symmetry, because the downwash figures do not change within a certain range in the transverse direction. Except for the peak, the curve resembles that of the rectangular and elliptical wing (reference 1) (fig. 18). A wide range of maximum values is distinctly noticeable in the pressure side flow, i.e., at negative  $\epsilon_h$  values, but not however - as would be expected on the basis of the calculation with a simple trailing

vortex (reference 1)\* - at approximately wing height and the drop of the downwash values toward both sides of the peak is, contrary to the theoretical curve for the simple trailing vortex, unsymmetrical and greater. The peak of the curve in figure 6 lies (dual-tube record) in vicinity of the stagnation point streamline as shown by a relative evaluation of the normal axis curves of the earlier measured elliptical wing (reference 1), which at the same time included a measurement of the position of the rear stagnation point streamline.

To establish the effect of finite wing chord on the downwash curves of the vertical axis (the same used in the earlier tests) (reference 1) the streamline pattern for airfoil No. 387 in two-dimensional flow was plotted according to the Kármán-Trefftz method (reference 6). The lift coefficient was  $c_a = 1.156$ , corresponding to the circulation at wing center with a mean  $c_a$  value of  $c_a = 1.0$  for a rectangular wing of 1:5 aspect ratio. The angles of downwash were taken from the streamline pattern. We also computed these for the same circulation

$$\Gamma = c_a \frac{v}{2} t$$

for the case of the lifting line. Referring the  $\epsilon_h$  and  $\epsilon_l$  values to a fictitious span of  $b = 5 t$  the expression then reads:

$$\alpha_w^0 = \frac{\epsilon_l \cdot 57.3}{\epsilon_h + \frac{10 \pi}{c_a} (\epsilon_h^2 + \epsilon_l^2)}$$

The result is shown in figure 15, where the angles of downwash for finite wing chord and the "lifting line" are plotted against  $\epsilon_h$ . The curves for the former are not as flat as those for the "lifting line" and drop asymmetricaly. They therefore resemble the experimental curves better

---

\*The formula on page 32 of reference 1 omits the factor 0.5 in the second term of the denominator, which conditions vertical axis asymmetry. But it does not affect the result.

especially in the proximity of the wing. But since they do not disclose a distinct range of maximum values on the pressure side, the asymmetrical course of the downwash values for greater wing distances still remains unexplained. So, if the simple trailing vortex substituted for the free vortex sheet and the finite wing chord fail to give the experimentally obtained variation of the downwash values, the only thing left is to revert to the vortex sheet. Any eventual rolling-up processes are provisionally considered subordinate. By "rolling-up" is meant, in accord with earlier reports (references 7, 8, and 9) primarily the movement, associated with the rolling up of the vortex sheet, of the inside lying free vortices away from the plane of symmetry of the wing toward the outside and of the inward motion of the vortices lying at the edge of the sheet up to the final concentration into two plain separate marginal vortices or vortex trains. This omission is made on the basis of the change in downwash magnitude by irregularities in lift distributions consistently observed in the present downwash studies even at greater distance behind the wing. This is particularly plain on the lateral axis curves of figure 5 (dual-tube record). The change in downwash value is especially pronounced for  $\epsilon_h = -0.2$ . The curve itself is unsymmetrical and undulatory. The fluctuations cannot be ascribed to the predetermined flow because it manifests no directional changes according to figure 16.\* It can be laid only to the given lift distribution, which in turn, owing to inaccuracies in model fabrication, itself becomes unsymmetrical. The inference that the rolling-up process or the lateral motion of the free vortices is subordinate was further concluded from the tests with propeller running as they manifested very distinctly, even at greater distance from the wing (near the tail) aside from the twist of the slipstream a range of nonuniformly changing downwash values extending to the right and left beyond the slipstream as compared to "wing alone."

Applying these facts to the downwash curves of the vertical axes (fig. 6) the following arguments may be advanced: since the outward motion of the free vortices in proximity of the plane of symmetry of the wing is negligible they can, by sufficient strength, because of their small distance from the plane of symmetry, develop a very pronounced effect upon

---

\*The smoother parallelism of the jet is probably due to the employment of the elliptical cone. The use of the earlier circular cone was accompanied by pronounced directional fluctuations.

the course of the downwash on the vertical axis lying in the plane of symmetry (argument advanced by H. Multhopp). These vortices near the plane of symmetry, moreover, lie, as a result of the sinking of the vortex sheet with the downwash, below the  $\epsilon_l$  axis and so produce the aforementioned one-sided range of high downwash coefficients.

Further, it may be stated that the marginal portions of the vortex sheet do not diminish in the same measure as the inside portions. The marginal vortices rather lie - as the earlier elliptical wing study (reference 1) also indicated - approximately at wing height. The maximum value of the downwash component due to the marginal vortices therefore lies about on the  $\epsilon_l$  axis (cf. reference 18).

The superposition of two assumedly separate theoretical downwash curves for marginal and inside vortices gives the actually unsymmetrical course of the curves, which, depending upon the strength of the marginal and inside vortices - affected by the lift distribution - is varyingly distinct.

According to the foregoing, a fairly good agreement obtains between the theoretical and experimental values when plotting a theoretical curve for a nonrolled-up vortex sheet and then shifting it approximately by the amount of the sinking of the vortex sheet.

Starting with a given lift distribution known from reference 10, 11, or 12 we obtain with

$$\alpha_w = \frac{w}{V + u} \quad \text{and} \quad k = \frac{\bar{\Gamma}}{\Gamma_0}$$

the following expression for the vertical axis in the plane of symmetry

$$\frac{\alpha_w}{\alpha_1} = \frac{\frac{2}{\pi} \int_0^1 \left\{ \frac{1}{\epsilon_h^2 + \xi^2} + \frac{\epsilon_l}{\sqrt{\epsilon_l^2 + \xi^2 + \epsilon_h^2}} \left( \frac{1}{\epsilon_h^2 + \xi^2} + \frac{1}{\epsilon_l^2 + \epsilon_h^2} \right) \right\} \frac{\partial}{\partial \xi} \frac{\Gamma}{\Gamma_0} d\xi}{1 + \frac{c_a}{k} \frac{F}{2\pi} \frac{1}{b^2} \int_0^1 \left( \frac{\epsilon_l}{(\epsilon_l^2 + \epsilon_h^2) \sqrt{\xi^2 + \epsilon_l^2 + \epsilon_h^2}} \right) \frac{\partial}{\partial \xi} \frac{\Gamma}{\Gamma_0} d\xi}$$

where

$\xi$  is current coordinate  $\frac{q}{b/2}$

$\Gamma$ , circulation at point  $\xi$

$\Gamma_0$ , circulation at wing center

$\bar{\Gamma}$ , mean circulation

$w$ , vertical interference velocity

$u$ , horizontal interference velocity

$V$ , wind velocity

The wing is assumed as lifting line.

The lift distribution of the given tapered wing was interpolated from the collected data of Fuchs and Hopf (reference 11) (fig. 17). The drop in lift distribution at the wing tip was approximated with

$$\frac{\Gamma}{\Gamma_0} = 1525 (1 - \epsilon_q)^{1/2}$$

within the limits  $\epsilon_q = 0.96$  to  $1.0$ , and the share of this range on the downwash computed by simple approximation (square terms disregarded). For the range of  $\epsilon_q = 0$  to  $0.20$  the lift distribution was approximated with

$$\frac{\Gamma}{\Gamma_0} = 1 - 0.875 \epsilon_q^2 \quad \text{and the integral within } \epsilon_q = 0 \text{ to } 0.96$$

was graphically defined. In view of the chosen high-distance factor  $\epsilon_l = 1.0$  the denominator term was put as before (reference 1) equal to 1.

The theoretical curve for nonrolled-up vortex sheet is shown in figure 6, with the computed curve shifted by the amount  $\epsilon_h = -0.2$ . The result is approximately the same as that obtained with the dual tube recorder at  $\alpha = 6.8^\circ$ , while the nondisplaced curve\* computed for the trailing

---

\*There is no cause for a displacement as the marginal vortices lie - as stated - at wing height. But shifting the downwash curve computed for the trailing vortex also by  $\epsilon_h = -0.2$ , affords, of course, a better agreement with the measured values, as the peaks of the curves then are at the same height.

vortex is not even approximately in accord with the experimental. This then explains the peak of the curves in figure 6.

Figure 18 shows the same for the previously measured elliptical wing (reference 1) at  $\alpha = 8.6^\circ$ . Since the position of its rear stagnation point streamline in the plane of symmetry had also been defined (wake measurement), the amount  $\Delta\epsilon_h$  of the reduction was thus known. It is  $\Delta\epsilon_h = -0.24$  according to figure 19 of reference 1. The peak or maximum value of the recorded downwash curve of the normal axis lies at  $\epsilon_h = -0.24$ , thus affording almost perfect agreement between peak position and height of vortex sheet. If the peak of the theoretical curve for nonrolled-up sheet is made to coincide with the peak of recorded downwash curve, then the shanks of the curves also coincide again approximately. The remaining discrepancies between the theoretical and experimental values of figures 6 and 18 are probably due to other than the different heights of marginal and inside vortices, to the necessary but still not quite exactly known correction factors for finite slipstream section for normal axes. Besides, the experimental value is higher as a result of the finite chord effect (fig. 16).

From the foregoing it is seen that comparatively good agreement obtains between theoretical and experimental values if the lateral displacements of the free vortices are neglected. The vertical displacements (sinking of vortex sheet), on the contrary, may not be disregarded. (This statement corrects the opposite assumption of the earlier report (reference 1)). To be sure, this applies only to the region of flow behind the inner part of a wing, that is, in the range of the tail.

Longitudinal axes.— This brings us to the discussion of the downwash factors measured on the longitudinal axes. Figure 19 presents the curves measured on longitudinal axes through the coordinate origin in plane of symmetry (dual-tube instrument) at different  $\alpha$ , along with the theoretical curves for the substitute trailing vortex ( $k = 0.74$ ) and an "upper" and "lower" limit similar to the original report (reference 1). Of course, the "upper" limit is not meant to be interpreted as in that report. There the "upper" limit in accord with Helmbold's report (reference 8) presented the values obtained with nonrolled-up vortex sheet and elliptical lift distribution. But now the "upper" limit applies to those values which are obtained

for nonrolled-up vortex sheet with the lift distribution belonging to predetermined wing. This step was taken since it became manifest that the "upper limit" of potential lift distributions on tapered wings can be considerably more remote from the trailing vortex curve than when distributed elliptically and fits the experimental values better.

How essential this difference is may be seen from figure 20, which presents the "upper limits" for the different lift distributions over the various wings. The expression for these curves reads:

$$\frac{\alpha_w}{\alpha_1} = \frac{2}{\pi} \int_0^1 \frac{1}{\xi} \left( 1 + \sqrt{1 + \frac{\xi^2}{\epsilon_l^2}} \right) \frac{\partial}{\partial \xi} \frac{\Gamma}{\Gamma_0} d\xi$$

The integral for  $\epsilon_q = 0$  to 0.96 was obtained graphically, that for  $\epsilon_q = 0.96$  to 1.0 mathematically. Figure 19 is very much like that obtained previously for the elliptical wing. Due to the fact that the nonrolled-up sheet affords the best actual values, provided the sinking of the vortex train is allowed for, a tolerable agreement of the measured curves with the "upper" limit must follow if, instead of the values at  $\epsilon_h = 0$  against  $\epsilon_l$  we plot the maximum values of these measured on the vertical axes. Plotting in figure 21 the maximum values of the normal axis downwash curves of all recorded angles of attack, it is seen that, as in figure 5, they lie in proximity of the upper limit curve.

Figure 22 presents the corresponding data for all angles of attack of the earlier elliptical wing study (reference 1). The greater the angle of attack is the closer, in both cases, the maximum experimental values with dual-tube recorder approach the "upper" limit. On the tapered wing, the difference is only about  $1^\circ$ , on the elliptical wing only about  $0.5^\circ$ . On the rectangular wing, it should be even less and on the wing with tapered lift distribution correspondingly higher.

Lateral axes.— As example of the measurements on the lateral axes of "wing alone" at  $\alpha = 6.8^\circ$ , see figure 5. The marked change in downwash in relation to  $\epsilon_q$  in contrast to the earlier measurements on the elliptical and

rectangular wing has already been pointed out. The lateral axis  $\epsilon_h = -0.2$  at  $\alpha = 6.8^\circ$  lies, as seen from figure 5, exactly at height of the maximum downwash values. Thus this lateral axis curve is comparable with a theoretical curve for nonrolled-up vortex sheet, because the lateral axis lies in the vortex sheet. The mathematical expression for it reads

$$\frac{\alpha_w}{\alpha_l} = \frac{1}{\pi} \int_0^1 \left\{ \frac{\sqrt{(\xi - \epsilon_q)^2 + \epsilon_l^2}}{\epsilon_l(\xi - \epsilon_q)} + \frac{2\xi}{\xi^2 - \epsilon_q^2} + \frac{\sqrt{(\xi + \epsilon_q)^2 + \epsilon_l^2}}{\epsilon_l(\xi + \epsilon_q)} \right\} \frac{\partial \Gamma}{\partial \xi} d\xi$$

This expression also was evaluated graphically.

Figure 5 shows - apart from the parallel displacement - the good agreement, thus proving anew that the lateral vortex motion during the rolling-up process plays no essential part.

#### b) Low-Wing Model with Ideal Fuselage

First we discuss the downwash on the "low wing with ideal fuselage," because the ideal fuselage influences the flow of the "wing alone" very little only, whence this arrangement with propeller running may, within a restricted angle of attack range, equally be termed "wing with propeller running," especially if reflecting that the propeller axis lies above the wing.

$\alpha = 3.15^\circ$ . - Figure 23 shows the results of eight lateral axes at distance  $\epsilon_l = 1.0$  for  $\alpha = 3.15^\circ$ . This angle  $\alpha = 3.15^\circ$  is distinguished by the fact that the propeller axis and the undisturbed flow direction are exactly coincident, that is, subject to a certain yaw only as a result of the upflow before the wing. The coefficient of advance is  $\lambda = 0.2$ . It also is

$$c_B = \frac{S}{\frac{\rho}{2} v^2 F_{prop}} = 0.34$$

if  $S$  is the drag difference of the reference polar and of the polar with  $\lambda = 0.2$ . The lift coefficient is  $c_a = 0.915$ . (The  $c_a$  values in text and diagrams refer to "wing alone" at the same  $\alpha$ .)

Taking the "reference measurements", "wing alone", and "wing with fuselage" by themselves, it is seen that the ideal fuselage has caused only on the lateral axis at pressure-side height  $\epsilon_h = -0.1$  a perceptible disturbance in downwash of "wing alone" while in the middle at this very height the fuselage produces no change in downwash.

The reason for the little influence of the ideal fuselage is that the lift distribution at  $\alpha = 3.15^\circ$  has been very little affected by the added fuselage.

The effect of propeller running is best presented by the lateral axis measurement at height  $\epsilon_h = 0.0$ . The slipstream twist in the downwash is plainly noticeable. The differences due to the twist are of about the same magnitude of  $\pm 4^\circ$ . The same is approximately true for the lateral axis curve at height  $\epsilon_h = -0.1$ , if it is assumed that the slipstream has removed the hole in the downwash distribution of the reference measurement "wing with fuselage" of this lateral axis (dashed part of the curve). On connecting (fig. 24) the centers of the zones of maximum and minimum downwash, the connecting line meets the plane of symmetry of the model about in point  $\epsilon_h = -0.03$ . This point should coincide with the slipstream center because there is scarcely a lateral movement of slipstream (cf. fig. 25).

From the accord of the  $\alpha_w$  points of the "reference model" and of the "model with propeller running" at  $\epsilon_q = 0$  (fig. 23) it may further be inferred that the slipstream center line at  $\alpha = 3.15^\circ$  and  $\lambda = 0.2$  adapts itself to the flow prescribed by the model without propeller. It is therefore neither sideways, upward, nor downward deflected. The answer to the question of validity for any other  $\lambda$  values or propeller loads is found in figure 25. According to it an increasing r.p.m. is followed by a slight lateral slipstream deflection to the left and - conformably to the rising circulation - downward. The opposite tendency is shown by the slipstream if the propeller windmills.

As to the course of the downwash on the lateral axis at height  $\epsilon_h = 0.0$ , that is, at height of slipstream axis, figure 23 further manifests: aside from the already mentioned zone in which - though reduced by the wide fuselage and the wing acting as guide apparatus - the twist of the slipstream occurs two other zones may be distinguished. They lie to the right and left of the slipstream approximately between  $\pm \epsilon_q = 0.14$  to  $0.45$ . In these transition zones there is a marked rise of downwash over the right half of the wing and a somewhat lesser downwash decrease over the left half. These deviations have therefore the opposite signs of those on the same half due to the twist. As the sense of rotation of the slipstream changes the deviations in the transition zones themselves change signs. The counter-rotating downwash changes to both sides of the slipstream are therefore directly related to the slipstream rotation (fig. 25).

The total downwash zone of the lateral axes disturbed by the propeller - that is, into which the disturbances enter as a result of the axial supplementary velocities in the slipstream - is on the average about twice as great as the propeller diameter, while according to Koning (reference 13) this zone should amount to about four times the propeller diameter. Strictly speaking the disturbed curve approaches the undisturbed curve asymptotically, although the limit can be fairly well gaged by the eye.

Mention should also be made of the attempt at simple qualitative derivation of this downwash distribution from the lift distribution modified by slipstream twist and supplementary axial slipstream velocity. But it was impossible to obtain an agreement between the theoretical and the experimental downwash distribution.

Figures 26 and 27 (vertical axes) complement figure 23. They indicate that the downwash changes relative to the reference curves on the pressure side are curiously still traceable at great distance from the wing, but disappear at shorter distance on the suction side. The same is seen in figure 28, which illustrates the angle of downwash at height  $\epsilon_h = \pm 0.2$  on two longitudinal axes in the plane of symmetry.

$\alpha = 6.8^\circ$ . - Figure 29 presents the results of downwash measurements on the lateral axes at distance  $\epsilon_l = 1.0$  for  $\alpha = 6.8^\circ$ . Hereby  $\lambda = 0.183$  and a correspondingly higher thrust coefficient than at  $\alpha = 3.15^\circ$ . It is  $c_g = 0.436$  and  $c_a = 1.18$ .

On comparing figure 28 with figure 29 it will be found that the curves, both the reference curves and those taken with propeller running are remarkably alike for the same height position, with exception of  $\epsilon_h = -0.2$ , for which the statement scarcely holds.

The latter might be associated with the fact that the height of  $\epsilon_h = -0.2$  at distance  $\epsilon_l = 1.0$  is exactly the height of the free vortex sheet (figs. 30 and 31; also fig. 6). The reference curve of "wing with fuselage" at height  $\epsilon_h = -0.2$  in figure 29 indicates jags within  $\epsilon_q = -0.25$  to  $+0.25$ , which probably are traceable to a nonuniform lift distribution over the wing roots or to the lateral keels of the fuselage-wing fillets. On this unstable curve the downwash changes, due to the slipstream effect, are built up. The last cited changes resemble those of the corresponding lateral axis curve at  $\alpha = 3.15^\circ$ , although at  $\alpha = 3.15^\circ$  the lateral axis for  $\epsilon_h = -0.2$  already lies below the free vortex sheet.

The similarity of the downwash curves of figures 23 and 29 is further restricted by the fact that at increasing  $\alpha$  the slipstream becomes smaller, as exemplified especially by the lateral axis curves for  $\epsilon_h = 0$  in figures 23 and 29. The reduction was at the expense of the right half of the superposition due to the twist. Figure 32 (lateral axis curves at  $\alpha = 10.6^\circ$ ) manifests the same phenomenon. It is probably associated with the increasing yaw of the propeller as  $\alpha$  is raised. With approximately horizontal propeller setting the right-side blade angle is smaller than that of the left-side blade, as a result of which the centroidal thrust distribution shifts toward the left (cf. fig. 25).

The downwash curves for the vortical axis in figures 30 and 31 do not confirm the statement made for  $\alpha = 3.15^\circ$ , namely, that the slipstream effect on the pressure side is still traceable at great distance away from the wing. Now it rather applies to the suction side, especially to the right half of the wing outside of the slipstream.

$\alpha = 10.6^\circ$ . - The lateral axis curves of figure 32 ( $\alpha = 10.6^\circ$ ,  $c_a = 1.411$ ,  $\lambda = 0.1655$ ,  $c_s = 0.642$ ) again disclose a certain resemblance - as already indicated - with the corresponding curves at  $\alpha = 3.15^\circ$  and  $\alpha = 6.8^\circ$ , although accompanied now by stronger deformations, in accordance with the approach to  $c_{a_{max}}$  and the pronounced yaw

of the propeller axis. At  $\epsilon_h = 0.0$  and  $\epsilon_h = -0.1$ , that is, relatively remote from the free vortex sheet, which itself lies at  $\epsilon_h = -0.255$ , the resemblance is still greatest both as regards the reference curves and the curves for the models with propeller running. But on approaching the free vortex sheet the reference curves as well as the downwash curves for the models with propeller running change quite considerably. If the symmetrical variation of the reference curve at  $\epsilon_h = -0.2$  is finally explainable with the markedly changed lift distribution due to the fuselage at great  $\alpha$  (reference 14) - a lift increase over the width of the fuselage may be deduced - an analysis of the downwash curve of the model with propeller running is scarcely possible yet for  $\epsilon_h = -0.255$  (free vortex sheet).

The vertical axis curves of figure 33 largely resemble those of figure 30, so that fundamentally they offer nothing new.

#### c) Low-Wing Model with Angular Fuselage

Figures 34 to 37 present the downwash curves for the lateral axis of the low-wing model with angular fuselage at  $\alpha = -0.6^\circ, 3.15^\circ, 6.8^\circ$ , and  $10.6^\circ$ . Comparing these first with those for the model with ideal fuselage we find: that the reference measurements of the low-wing models without propeller running differ considerably, as soon as they are not too far away from the free vortex sheet, even while  $\alpha$  is still low. While on the low-wing model with ideal fuselage - apart from the greatest angle of attack  $\alpha = 10.6^\circ$ , where the downwash increases over a small region - the downwash is substantially the same as on "wing alone" - the fuselage of the low-wing model with angular body manifests a marked decrease in downwash over a comparatively great width. At the same time a very small but particularly deep zone - for example at  $\alpha = 3.15^\circ, 6.8^\circ$ , and  $10.6^\circ$  for  $\epsilon_h = 0.0$  - is repeatedly noted next to the usually comparatively wide and deep upwind zone (as against "wing alone").

Figure 38 presents the downwash values of all reference measurements for the plane of symmetry and  $\epsilon_h = 0$ . At this height only  $\alpha = 10.6^\circ$  is without abnormal change relative to "wing alone" because at  $\alpha = 10.6^\circ$ ,  $\epsilon_h = 0$  is very remote from the vortex sheet.

Examining the reference measurements of the higher  $\alpha$

in figures 36 and 37, lying approximately at  $\epsilon_h = -0.255$  (level of vortex sheet) - at  $\alpha = 6.8^\circ$  it lies at  $\epsilon_h = -0.2$ , at  $\alpha = 10.6^\circ$  at  $\epsilon_h = -0.26$  - the change in downwash approximates  $7^\circ$  to  $8^\circ$  as compared to "wing alone" while these discrepancies are surprisingly uniformly distributed over a range from  $\epsilon_q = -0.175$  to  $\epsilon_q = +0.175$ . Farther away from the vortex sheet this distribution is not so sharp, but rather more equalized.

The portrayed downwash distribution of the reference curves is again subject to the effects caused by the propeller running. The differences between "reference measurements" and those with "propeller running" are quite similar on both models for lateral axes not too close to the vortex train. Although this resemblance is not general, it can be observed repeatedly, for example, at  $\alpha = 3.15^\circ$  with  $\epsilon_h = 0.0$  or  $-0.1$ , at  $\alpha = 6.8^\circ$  with  $\epsilon_h = 0$  or  $\pm 0.1$  and at  $\alpha = 10.6^\circ$  with  $\epsilon_h = 0$  or  $-0.1$ . If, however, the lateral axes are on a level with the vortex surface, there is neither similarity of the course of discrepancies nor of the downwash curves with propeller running. This might be associated with a filling up of a vortex sink through the running propeller caused by the angular fuselage in the lift distribution of the low-wing model. This might also account for the greater average supplementary downwash values on the model with propeller running (section D, II, 3).

The measurements on lateral axes with  $\epsilon_h = 0$  at different revolutions (figs. 39 to 42) disclose in contrast to figure 25 (low-wing model with ideal fuselage,  $\alpha = 3.15^\circ$ ), that the changes to right next to the zone of twist are surprisingly small. At the left they disappear altogether, while in figure 25 at least a slight change could be detected.

The vertical axis measurements at  $\alpha = 6.8^\circ$  in figures 43 and 44 manifest similarity with the corresponding measurement only on the left-hand side ( $\epsilon_q = -0.12$ ) of the model with ideal fuselage (fig. 30).

The plot of the "lines of equal angle of downwash" of the low-wing model with angular fuselage at  $\alpha = 6.8^\circ$  (fig. 45) resembles that of the model with ideal fuselage (fig. 24,  $\alpha = 3.15^\circ$ ). From the plot, figure 45, together with figure 1 (side view of low-wing model) it is again observed

that the slipstream adapts itself in some fashion to the flow pattern prescribed by the wing.

The longitudinal axis measurements at  $\alpha = 6.8^\circ$  (figs. 46 and 47) resemble those of the model with ideal fuselage (fig. 28) at  $\alpha = 3.15^\circ$ .

### 3. Magnitude of Mean Supplementary Downwash

#### Due to Propeller Slipstream

So far the argument did not include the resultant mean values of the downwash, whereas the supplementary downwash values, especially those caused by propeller running, are of special significance.

$\epsilon_q = -0.3$  to  $\epsilon_q = +0.3$ . - Figure 48 presents for the "low-wing model with ideal fuselage" the planimetrically obtained mean downwash values  $\overline{\Delta \alpha_w}$  of the lateral axis curves with  $\epsilon_h = 0.0$  for the range of  $\epsilon_q = -0.3$  to  $+0.3$  plotted against  $\lambda$ ,  $c_s$ , and  $c_a$ , with the parameters  $\alpha$ ,  $\alpha$ , and  $\lambda$ .

Beginning with curve  $\overline{\Delta \alpha_w} = f(\lambda)$  and parameter  $\alpha = 3.15^\circ$ , the 5 test points - 1 at zero thrust, another with decelerated propeller - lie except for minor scattering on a straight line. The latter is drawn so as to give at  $\lambda = 0.296$  - the  $\lambda$  value for zero thrust according to the drag measurements of figure 7 - zero supplementary downwash. Hence the one-sided scatter of the points at zero thrust and in the decelerated zone. The choice of location of the straight line is perhaps not altogether correct, as it also is conceivable that with zero outward thrust the propeller actually produces thrust, but which is absorbed by the increased drag induced by the slipstream. Aside from the point "zero thrust" that for "torque equal to zero" is also essential. The curve must apparently lie between the two points. But as the scatter - at least within the range of

$\overline{\Delta \alpha_w} = 0$  - remains within measuring accuracy, we proceeded in the described manner. The straight lines were drawn through the same point with the coordinates  $\overline{\Delta \alpha_w} = 0$  and  $\lambda = 0.296$  for  $\overline{\Delta \alpha_w} = f(\lambda)$  with the parameters  $\alpha = 6.8^\circ$  and  $10.6^\circ$ . These straight lines allow a convenient and admissible extrapolation in the climbing flight range, or at

around  $\lambda = 0.14$  with the prescribed propeller. Then, as is seen, at  $\alpha = 6.8^\circ$  - approximately resembling the angle of attack for climb - the supplementary downwash amounts to only about  $0.80^\circ$ . Here  $c_g = 0.8$ . This  $0.80^\circ$  corresponds to 10 percent of the prescribed average for the reference model "wing with fuselage."

The supplementary mean angle of downwash  $\overline{\Delta\alpha_w}$  was also plotted for  $\lambda = 0.15$  and  $\lambda = 0.2$  as parameter against the lift  $c_a$  of the model "wing with fuselage and propeller running." The relation observed in the explored  $c_a$  range is again approximately linear. The sharp rise of  $\overline{\Delta\alpha_w}$  with increasing  $c_a$  is probably associated with the simultaneously increasing tilt of the propeller axis.

The curves  $\overline{\Delta\alpha_w} = f(c_g)$  are slightly parabolic.

Figure 49 presents the same pictures as figure 47 for the low-wing model with angular fuselage. On the latter model the supplementary  $\overline{\Delta\alpha_w}$  values are materially increased through the running propeller, even though it is still far from the order of magnitude arrived at by another source (reference 15). With  $\lambda = 0.14$  the supplementary angle of downwash is  $\overline{\Delta\alpha_w} = 1.5^\circ$  at maximum  $\alpha$ . As to figure 49, it should be noted that at small  $\alpha$  the departure from the plotted curves is especially great. The measurements are not extensive enough to permit of more accurate predictions for small  $\alpha$ .

Figures 50 and 51 indicate the manner in which the supplementary downwash created by the slipstream is governed by the height level of the tail. The peak of the curves lies approximately on a level with the free vortex sheet.

#### 4. Total Mean Angle of Downwash

Supplementary to figures 50 and 51, figures 52 and 53 show the mean angle of downwash of the reference models plotted against the height level of the tail. It will be noted that in stability studies the height level of the tail is apparently of prime importance (cf. section F).

Figure 54 shows the mean angle of downwash for all reference measurements, averaged for  $\epsilon_q = -0.3$  to  $+0.3$  against  $\alpha$ , and thus illustrates the "body effect, the tail

being always at level  $\epsilon_h = 0.0$  (wind-axis system). It particularly reveals that the ideal fuselage within the studied  $\alpha$  range creates a small additional downwash as compared to "wing alone" and the angular fuselage a fairly strong upwind.

Figures 55 and 56 show the total mean angle of downwash for both low-wing models plotted against  $\alpha$  with the parameters  $\lambda = 0.15$  and  $0.2$ .

Figures 57 and 58 bring the same presentations of  $\alpha_w$  with the parameters  $c_w = 0$  and "full throttle." An identical "full throttle polar" as shown by dotted curve in figures 13 and 14 was assumed.\* The curves for  $c_w = 0$  and full throttle are not materially different.

#### 5. Comparison of the Mean Downwash as Obtained by Detector and Point-by-Point Measurement

For the case of downwash distribution as exemplified by the low-wing model with angular fuselage (without propeller running at  $\alpha = 10.6^\circ$  and  $\epsilon_h = -0.2$  (fig. 37), the mean angle of downwash as would be obtained with a rectangular detector vane of aspect ratio  $\frac{t_H}{b_H} = 1:3$  (1:4) and span  $b_H = 0.3 b$  (0.4 b), was determined mathematically. The calculation followed Muthopp's method of lift distribution calculus under the assumption that the change in wind direction can be equated to a twist of the detector vane and that the air speed is constant. The results were as follows:

| Planimetrically defined mean value of the prescribed (measured) downwash distribution | $\frac{b_H}{b}$ | $\frac{t_H}{b_H}$ | Mean downwash as computed with detector vane |
|---|-----------------|-------------------|--|
| 6.83°   | 0.3             | 1:3               | 6.16°  |
| 7.58°   | 0.4             | 1:4               | 7.31°  |

\*The full throttle polars in figures 13 and 14 present only approximate values.

Measurement with detector vane accordingly gives a lower figure than with point-by-point measurement. In a comparison of angles of downwash defined according to different test method this fact should be borne in mind.

#### E. VELOCITY DISTRIBUTION IN THE SLIPSTREAM

Figures 59 to 61 show the velocity distribution in the slipstream of the low-wing model with angular fuselage at  $\alpha = 6.8^\circ$  and the coefficient of advance  $\lambda = 0.1865$  at  $\epsilon_l = 1.0$ . Again the lateral axis measurement indicates a stronger thrust on the left than on the right-hand side. The slipstream center lies approximately at  $\epsilon_h = 0.03$ . Figure 62 illustrates the velocity distribution averaged over the range of  $\epsilon_q = -0.3$  to  $+0.3$  against  $\epsilon_h$ . The horizontal tail surfaces of an airplane on passing through the slipstream are, if the angle of attack is changed, on the average in a wind of constant mean dynamic pressure, unless they reach the jet boundary or emerge from it.

In the velocity distribution test, the static pressure was measured separately from the total head. For the latter, a pitot-venturi was used of directional insensitivity within a range of  $\pm 45^\circ$ . The static tube was turned into the previously measured flow direction.

Our velocity distribution measurements in the slipstream were confined to the low-wing model with angular fuselage and  $\alpha = 6.8^\circ$  and  $\lambda = 0.1865$ , although for stability studies (section F), the knowledge of the additional velocity in the slipstream - whose mean value referred to lateral tail axis is according to figure 62, approximately unaffected by the height level of the tail - of both models and at several  $\alpha$  and  $\lambda$  is necessary. These additionally needed values were mathematically approximated on the basis of an assumed dependence of  $\lambda$  but not of  $\alpha$  or the model form.

The additional axial velocity in the slipstream far downstream from the propeller is

$$\frac{w}{v} = \frac{k_B(1 + 2\lambda)}{2\lambda^4 \left[ \frac{1}{\lambda^2} - \ln \left( 1 + \frac{1}{\lambda^2} \right) \right]}$$

for a "propeller with minimum energy loss" (reference 16). This formula is indicated by the curve (1) in figure 63. The dependence of  $\lambda$  and  $k_g$  being assumed as shown in figure 4 on the basis of the polar measurement (dotted curve). Through the mean value of  $\frac{q_{HL}}{q_0}$  obtained for the low-wing model with angular fuselage at  $\alpha = 6.8^\circ$  and  $\lambda = 0.1865$  we then drew a curve which results from affine variation of curve (1). The ensuing curve (2) presents approximately the dependence of  $\frac{q_{HL}}{q_0}$  on  $\lambda$  for the investigated low-wing models.

#### F. APPLICATION OF THE RESULTS TO STABILITY INVESTIGATIONS

In a statically longitudinally stable airplane, the horizontal tail surfaces must, if the angle of attack of the airplane is changed, produce a restoring moment, that is,  $\frac{dM}{d\alpha}$  must be positive. The moment is

$$M_{HL} = c_{HL} \frac{q_{HL}}{q_0} \text{ const.}$$

with

$$c_{HL} = (\alpha_{aer} - \alpha_w + \beta)$$

as the angle of attack of the horizontal tail surface, if  $\alpha_{aer}$  represents the angle of attack of the wing referred to zero lift direction and the zero lift direction of the horizontal tail surfaces relative to the zero lift direction of the wing has  $\beta$  as angle of setting. The criterion for the stability then reads as

$$\frac{dM}{d\alpha} = \left( 1 - \frac{d\alpha_w}{d\alpha} \right) \frac{q_{HL}}{q_0}$$

provided  $\frac{q_{HL}}{q_0} = \text{const.}$

This factor  $\frac{q_{HL}}{q_0}$  is constant if  $\lambda$  is a constant, for example, for the "reference measurement" at which  $\frac{q_{HL}}{q_0}$  may be put = 1.

Considering, on the contrary, polars with the parameters " $c_w = 0$ " and "full throttle" then  $\frac{q_{HL}}{q_0} > 1$  and equally dependent on  $\alpha$ . The procedure in these cases was to put  $\frac{q_{HL}}{q_0} = 1$  and use a smaller angle of downwash  $\alpha_w^*$  which in a way produces the actually greater returning moment. The expression for  $\alpha_w^*$  reads:

$$\alpha_w^* = \alpha_{aer} - \alpha_{HL} \frac{q_{HL}}{q_0}$$

or

$$\alpha_w^* = \alpha_{aer} - (\alpha_{aer} - \alpha_w + \beta) \frac{q_{HL}}{q_0} = (\alpha_w - \beta) \frac{q_{HL}}{q_0}$$

Now the stability criterion reads as

$$\frac{d M}{d \alpha} = 1 - \frac{d \alpha_w^*}{d \alpha}$$

It should be observed that the height level of the tail is different at the different angles of attack. In the following example, it is assumed at  $\epsilon_n = +0.1$  for  $\alpha = 0^\circ$ . Every angle of attack has a different  $\epsilon_h$  fixed in wind direction. Figures 50 to 53, which show  $\epsilon_q$  by dot and dash can be used to establish the relation of  $\frac{\Delta \alpha_w}{\lambda}$  to  $\lambda$  (and  $c_a$ ) (figs. 64 and 65) from which the related values of  $\alpha_w$  and  $\alpha$  for body-fixed horizontal tail

surfaces with parameters  $\lambda = \text{const.}$ ,  $c_w = 0$  and full throttle may be read. The related  $\lambda$  value of any other pair of values was obtained from the polar diagrams or from figures 7 and 10. In both tail arrangements, the horizontal tail surface does not move out of the slipstream as a closer examination of the lateral axis downwash curves disclosed (figs. 23, 29, 32, 34 to 37), so that at last with the  $\frac{q_{HL}}{q_0}$  values of figure 62 the graphs of the relationship between  $\alpha_w^*$  and  $\alpha$  could be developed.

Figure 66 presents such a graph for the low-wing model with angular fuselage and body-fixed tail.

Figure 67 shows  $\frac{dM}{d\alpha} = f(\alpha)$ . For comparison the stability values  $\frac{dM}{d\alpha}$  were plotted also for constant  $\epsilon_h = 0$  (fig. 68). This arrangement is termed "wind-fixed" as against the normal "body-fixed" system. The graphs disclose the following:

- a) On a wind-fixed horizontal tail surface, the  $\frac{dM}{d\alpha}$  values are usually higher than on one that is body-fixed. This result can be explained with the fact that with wind-fixed arrangement the horizontal tail surface is far removed from the vortex sheet and this distance increases with the angle of attack.
- b) For wind-fixed horizontal tail surface, all curves - so long as  $c_{a_{max}}$  is not approached - lie above the reference curve; or in other words, there is in every case a stability gain relative to the reference model. On approaching  $\alpha_{max}$  the curve for "full throttle" drops below the reference curve, but then very considerably. On the body-fixed horizontal tail surface on the other hand, the likewise very steep, full-throttle curve meets the reference curve at a much lower angle of attack ( $\alpha = 6.8^\circ$ ); then the stability is deficient in the climbing range.

From this it becomes apparent that the stability of an airplane can be improved if, in order to change the angle of attack, the wing is rotated with respect to the body rather

than the whole airplane.\* It is possible that on account of the unchanged position of fuselage and slipstream a further improvement in stability can be effected, because with running propeller a portion of the additional downwash is probably due to the turning of the slipstream and the lift distribution at greater wing incidence relative to the fuselage acts with increasing  $\alpha$  in the sense of a downwash reduction - through the created sink in the lift distribution.

Figure 69 presents the change in pitching moment of the low-wing model with ideal fuselage for the case of body-fixed horizontal tail surface.

This presentation affords a comparison of the two low-wing models as regards stability (figs. 67 and 69). The reference measurements give an appreciably higher stability to the model with angular fuselage. The curves with the parameters " $c_w = 0$ " and " $\lambda = \text{const.} = 0.1865$ " manifest no radical departure. Thus the drawback of the ideal fuselage in the comparison of the reference measurements is approximately neutralized again. But for the full-throttle polar the model with angular fuselage is distinctly superior, especially at large angles of attack. This finding which is in accord with experience in actual practice (reference 17) is particularly remarkable in view of the fact that the additional angle of downwash  $\Delta \alpha_w$  due to the slipstream is greater on the model with angular fuselage than on that with ideal fuselage. It is also worthy of note that an identical pair of values of  $c_a$  and  $c_w$  on the different low-wing models had a different  $\lambda$  and  $k_s$  value. In other words: the greater stability of the model with angular fuselage is obtained at the expense of power loss. The same holds true for the models without propeller running, as seen from the polars of figures 2, 13, and 14.

Translation by J. Vanier,  
National Advisory Committee  
for Aeronautics.

---

\*The effect of angle-of-attack change could also be produced by slots and flaps on wings moved about the spar axis instead of with respect to the fuselage. Perhaps a slotted wing might be developed whose slots would be merely turned in place of an elevator deflection.

## REFERENCES

1. Muttray, H.: Untersuchungen über die Grösse des Abwindes hinter Tragflügeln mit rechteckigem und elliptischem Umriss. Luftfahrtforschung; vol. 12, no. 8, 1935, p. 28.
2. Hueber, J.: Die aerodynamischen Eigenschaften von Doppeltrapezförmigen Tragflügeln. Z.F.M., vol. 24, no. 10, p. 249.
3. Muttray, H.: The Aerodynamic Aspect of Wing-Fuselage Fillets. T.M. No. 764, N.A.C.A., 1935.
4. Durand, W. F., and Lesley, E. P.: Experimental Research on Air Propellers - V. T.R. No. 141, N.A.C.A., 1922.
5. Lotz, I.: Correction of Downwash in Wind Tunnels of Circular and Elliptic Sections. T.M. No. 801, N.A.C.A., 1936.
6. Von Kármán, Th., and Trefftz, E.: Potentialströmung um gegebene Tragflügelquerschnitte. Z.F.M., Sept. 28, 1918, p. 111.
7. Prandtl, L.: Tragflügeltheorie, II. Mitteilung, L. Prandtl und A. Betz. Vier Abhandlungen zur Hydrodynamik und Aerodynamik, Göttingen 1927, p. 80 (Auslieferung durch den Verlag Julius Springer, Berlin.)
8. Helmbold, H. B.: Über die Berechnung des Abwindes hinter einem rechteckigen Tragflügel. Z.F.M., vol. 16, 1925, p. 291.
9. Kaden, H.: Aufwicklung einer unstabilen Unstetigkeitsfläche. Ingenieur-Archiv, vol. 2, no. 2, 1931, p. 141.
10. Lotz, I.: Berechnung der Auftriebsverteilung beliebig geformter Flügel. Z.F.M., vol. 22, no. 7, 1931, p. 189.
11. Fuchs, R., Hopf, L., and Seewald Fr.: Aerodynamik, vol. II, chap. 6, (Verlag Julius Springer, Berlin, 1935).

12. Lippisch, A.: Method for the Determination of the Spanwise Lift Distribution. T.M. No. 778, N.A.C.A., 1935.
13. Koning, C.: Influence of the Propeller on other Parts of the Airplane Structure, Aerodynamic Theory, by F. W. Durand, vol. 4, p. 411, fig. 17. Julius Springer, Berlin, 1935.
14. Vladea, Joan: Effect of Fuselage and Engine Nacelles on Some Aerodynamic Properties of an Airplane Wing. T.M. No. 736, N.A.C.A., 1934.
15. Bradfield, F. B.: Wind Tunnel Data on the Effect of Slipstream on the Downwash and Velocity at the Tailplane. R. & M. No. 1488, British A.R.C., 1932.
16. Betz, A.: Tragflügel und Flügelräder. Hütte I, 26. Afl. p. 405.
17. Hibbert, L.: Das Schnellflugzeug: Entwicklung und Zielsetzung. Luftwissen, vol. 2, 1935, p. 272.
18. Lotz, I., and Fabricius, W.: Die Berechnung des Abwindes hinter einem Tragflügel bei Berücksichtigung des Aufwickelns der Unstetigkeitsfläche. Luftfahrtforschung, vol. 14, 1937, p. 533.

## LEGENDS

- Figure 1.- Investigated forms of wings and fuselages.
- Figure 2.- Polars of the figure 1 models without propeller.
- Figure 3.- The employed 2-blade propeller.
- Figure 4.- Propeller performance characteristics.
- Figure 5.- Downwash on superposed lateral axes in tail proximity (theory and different test methods).
- Figure 6.- Downwash on a vertical axis in proximity of the tail (theory and various test methods).
- Figure 7.- Drag coefficients of low-wing model with ideal fuselage and propeller running.
- Figure 8.- Lift coefficients of model with ideal fuselage and propeller running.
- Figure 9.- Pitching moment coefficient of model with ideal fuselage and propeller running.
- Figure 10.- Drag coefficients of model with angular fuselage and propeller running.
- Figure 11.- Lift coefficients of model with angular fuselage and propeller running.
- Figure 12.- Pitching-moment coefficients of model with angular fuselage and propeller running.
- Figure 13.- Polars for model with ideal fuselage and propeller running.
- Figure 14.- Polars of low-wing model with angular fuselage and propeller running.
- Figure 15.- Effect of finite wing chord on downwash.
- Figure 16.- Directional changes within the open jet of the "small tunnel" of the AVA, Göttingen (elliptical cone).
- Figure 17.- Lift distribution of the studied quasi-taper wing.
- Figure 18.- Downwash on a vertical axis of the elliptical wing of earlier tests (reference 1).

- Figure 19.- Downwash on longitudinal axis near the plane of symmetry (dual-tube record).
- Figure 20.- Upper limit of downwash for different wing contours.
- Figure 21.- Maximum downwash on tapered wing (dual-tube record).
- Figure 22.- Maximum downwash on elliptical wing in earlier test (reference 1). (Dual-tube record.)
- Figure 23.- Angle of downwash on lateral axes at different height levels (low-wing model with ideal fuselage and propeller running;  $\alpha = 3.15^\circ$ ;  $c_a = 0.915$ ;  $\epsilon_l = 1.0$ ;  $\lambda = 0.203$ ).
- Figure 24.- Lines of equal angle of downwash (low-wing model, ideal fuselage, propeller running;  $\alpha = 3.15^\circ$ ;  $c_a = 0.915$ ;  $\epsilon_l = 1.0$ ;  $\lambda = 0.203$ ).
- Figure 25.- Angle of downwash on the lateral axis at height level of wing for different coefficients of advance (low-wing model, ideal fuselage, propeller running;  $\alpha = 3.15^\circ$ ;  $c_a = 0.915$ ;  $\epsilon_l = 1.0$ ;  $\epsilon_h = 0$ ).
- Figure 26.- Angle of downwash on a vertical axis in plane of symmetry (model with ideal fuselage and propeller running;  $\alpha = 3.15^\circ$ ;  $c_a = 0.915$ ;  $\epsilon_l = 1.0$ ;  $\epsilon_q = 0$ ;  $\lambda = 0.203$ ).
- Figure 27.- Angle of downwash on two vertical axes through the slipstream (model with ideal fuselage and propeller running;  $\alpha = 3.15^\circ$ ;  $c_a = 0.915$ ;  $\epsilon_l = 1.0$ ;  $\lambda = 0.203$ ).
- Figure 28.- Angle of downwash on two longitudinal axes in plane of symmetry (model with ideal fuselage and propeller running;  $\alpha = 3.15^\circ$ ;  $c_a = 0.915$ ;  $\epsilon_q = 0$ ;  $\lambda = 0.203$ ).
- ✓ Figure 29.- Angle of downwash on lateral axes at different height levels (model with ideal fuselage and propeller running;  $\alpha = 6.8^\circ$ ;  $c_a = 1.18$ ;  $\epsilon_l = 1.0$ ;  $\lambda = 0.183$ ).
- Figure 30.- Angle of downwash on two vertical axes through the slipstream (model with ideal fuselage and propeller running;  $\alpha = 6.8^\circ$ ;  $c_a = 1.18$ ;  $\epsilon_l = 1.0$ ;  $\lambda = 0.183$ ).
- Figure 31.- Angle of downwash on two vertical axes through

the disturbed downwash zones left and right of slipstream (model with ideal fuselage and propeller running;  $\alpha = 6.8^\circ$ ;  $c_a = 1.18$ ;  $\epsilon_l = 1.0$ ;  $\lambda = 0.183$ ).

✓ Figure 32.- Angle of downwash on lateral axes at different height levels (model with ideal fuselage, propeller running;  $\alpha = 10.6^\circ$ ;  $c_a = 1.411$ ;  $\epsilon_l = 1.0$ ;  $\lambda = 0.1655$ ).

Figure 33.- Angle of downwash on two vertical axes through the slipstream (model with ideal fuselage and propeller running;  $\alpha = 10.6^\circ$ ;  $c_a = 1.411$ ;  $\epsilon_l = 1.0$ ;  $\lambda = 0.1655$ ).

✓ Figure 34.- Angle of downwash on lateral axes at different height levels (model with ideal fuselage, propeller running;  $\alpha = -0.6^\circ$ ;  $c_a = 0.635$ ;  $\epsilon_l = 1.0$ ;  $\lambda = 0.222$ ).

✓ Figure 35.- Angle of downwash on lateral axes at different position levels (low-wing model with angular fuselage and propeller running;  $\alpha = 3.15^\circ$ ;  $c_a = 0.915$ ;  $\epsilon_l = 1.0$ ;  $\lambda = 0.206$ ).

✓ Figure 36.- Angle of downwash on lateral axes at different position levels (low-wing model with angular fuselage and propeller running;  $\alpha = 6.8^\circ$ ;  $c_a = 1.18$ ;  $\epsilon_l = 1.0$ ;  $\lambda = 0.1885$ ).

✓ Figure 37.- Angle of downwash on lateral axes at different position levels (low-wing model with angular fuselage and propeller running;  $\alpha = 10.6^\circ$ ;  $c_a = 1.411$ ;  $\epsilon_l = 1.0$ ;  $\lambda = 0.1705$ ).

Figure 38.- Amount of angle of downwash in a point of the plane of symmetry at wing level of the models without propeller running ( $\epsilon_h = 0$  (wind-fixed);  $\epsilon_l = 1.0$ ).

✓ Figure 39.- Angle of downwash on lateral axis at wing level for different coefficients of advance (low-wing model, angular fuselage and propeller running;  $\alpha = -0.6^\circ$ ;  $c_a = 0.635$ ;  $\epsilon_l = 1.0$ ;  $\epsilon_h = 0$ ).

✓ Figure 40.- Angle of downwash on lateral axis at wing level for different coefficients of advance (low-wing model, angular fuselage and propeller running;  $\alpha = 3.15^\circ$ ;  $c_a = 0.915$ ;  $\epsilon_l = 1.0$ ;  $\epsilon_h = 0$ ).

✓ Figure 41.- Angle of downwash on lateral axis at wing level for different coefficients of advance (low-wing model, angular fuselage and propeller running;  $\alpha = 6.8^\circ$ ;  $c_a = 1.18$ ;  $\epsilon_l = 1.0$ ;  $\epsilon_h = 0$ ).

Figure 42.- Angle of downwash on lateral axis at wing level for different coefficients of advance (low-wing model, angular fuselage, and propeller running;  $\alpha = 10.6^\circ$ ;  $c_a = 1.411$ ;  $\epsilon_l = 1.0$ ;  $\epsilon_h = 0$ ).

Figure 43.- Angle of downwash on a vertical axis in the plane of symmetry (low-wing model, angular fuselage, and propeller running;  $\alpha = 6.8^\circ$ ;  $c_a = 1.18$ ;  $\epsilon_q = 0$ ;  $\lambda = 0.1885$ ).

Figure 44.- Angle of downwash on two vertical axes through slipstream (low-wing model, angular fuselage, and propeller running;  $\alpha = 6.8^\circ$ ;  $c_a = 1.18$ ;  $\epsilon_l = 1.0$ ;  $\lambda = 0.1885$ ).

Figure 45.- Lines of equal angle of downwash (low-wing model, angular fuselage, and propeller running;  $\alpha = 3.8^\circ$ ;  $c_a = 1.18$ ;  $\epsilon_l = 1.0$ ;  $\lambda = 0.1885$ ).

Figure 46.- Curve of angle of downwash on two longitudinal axes in plane of symmetry (low-wing model, angular fuselage, and propeller running;  $\alpha = 6.8^\circ$ ;  $c_a = 1.18$ ;  $\epsilon_q = 0$ ;  $\lambda = 0.1885$ ).

Figure 47.- Angle of downwash on two longitudinal axes at wing level through the propeller slipstream (low-wing model, angular fuselage, and propeller running;  $\alpha = 6.8^\circ$ ;  $c_a = 1.18$ ;  $\epsilon_h = 0$ ;  $\lambda = 0.1885$ ).

Figure 48.- Mean additional angle of downwash created by the slipstream (low-wing model, ideal fuselage, and propeller running;  $\epsilon_h = 0$  (wind-fixed);  $\epsilon_l = 1.0$ ;  $\epsilon_q$  from  $-0.3$  to  $+0.3$ ).

Figure 49.- Mean additional angle of downwash created by the slipstream (low-wing model, angular fuselage, and propeller running;  $\epsilon_h = 0$  (wind-fixed);  $\epsilon_l = 1.0$ ;  $\epsilon_q$  from  $-0.3$  to  $+0.3$ ).

Figure 50.- Mean additional angle of downwash due to slipstream against tail level (low-wing model with ideal fuselage and propeller running).

Figure 51.- Mean additional angle of downwash due to slipstream against tail level (low-wing model with angular fuselage and propeller running).

Figure 52.- Mean angle of downwash of low-wing model with-

out propeller against height level of tail (low-wing model with ideal fuselage;  $\epsilon_l = 1.0$ ;  $\epsilon_q$  from  $-0.3$  to  $+0.3$ ; reference measurement).

Figure 53.- Mean angle of downwash of low-wing model without propeller against height level of tail (low-wing model with angular fuselage;  $\epsilon_h = 1.0$ ;  $\epsilon_q$  from  $-0.3$  to  $+0.3$ ; reference measurement).

Figure 54.- Mean angle of downwash of low-wing model without propeller against  $\alpha$  ( $\epsilon_h = 0$  (wind-fixed);  $\epsilon_l = 1.0$ ;  $\epsilon_q$  from  $-0.3$  to  $+0.3$ ).

Figure 55.- Mean angle of downwash of low-wing model with propeller running against  $\alpha$  (low-wing model ideal fuselage  $\epsilon_h = 0$ , wind-fixed;  $\epsilon_l = 1.0$ ;  $\epsilon_q$  from  $-0.3$  to  $+0.3$ ).

Figure 56.- Mean angle of downwash of low-wing model with propeller running against  $\alpha$  (low-wing model, angular fuselage;  $\epsilon_h = 0$  (wind-fixed);  $\epsilon_l = 1.0$ ;  $\epsilon_q$  from  $-0.3$  to  $+0.3$ ).

Figure 57.- Mean angle of downwash of low-wing model with propeller running against  $\alpha$  (low-wing model, ideal fuselage,  $\epsilon_h = 0$  (wind-fixed);  $\epsilon_l = 1.0$ ;  $\epsilon_q$  from  $-0.3$  to  $+0.3$ ).

Figure 58.- Mean angle of downwash of low-wing model with propeller running against  $\alpha$  (low-wing model, angular fuselage;  $\epsilon_h = 0$  (wind-fixed);  $\epsilon_l = 1.0$ ;  $\epsilon_q$  from  $-0.3$  to  $+0.3$ ).

Figure 59.- Velocity distribution in slipstream (low-wing model, angular fuselage, propeller running;  $\alpha = 6.80^\circ$ ;  $c_a = 1.18$ ;  $\epsilon_l = 1.0$ ;  $\epsilon_h = 0$ ;  $\lambda = 0.1865$ ).

Figure 60.- Velocity distribution in slipstream (low-wing model, angular fuselage, propeller running;  $\alpha = 6.80^\circ$ ;  $c_a = 1.18$ ;  $\epsilon_l = 1.0$ ;  $\epsilon_q = 0$ ;  $\lambda = 0.1865$ ).

Figure 61.- Lines of equal velocity slipstream (low-wing model with angular fuselage and propeller running;  $\alpha = 6.8^\circ$ ;  $c_a = 1.18$ ;  $\epsilon_l = 1.0$ ;  $\lambda = 0.1865$ ).

Figure 62.- Mean dynamic pressure distributed in slipstream

(low-wing model, angular fuselage, propeller running;  
 $\alpha = 8.8^\circ$ ;  $c_a = 1.18$ ;  $\epsilon_l = 1.0$ ;  $\lambda = 0.1865$ ).

Figure 63.- Supplementary axial velocity in slipstream.

Figure 64.- Mean additional angle of downwash due to slipstream (low-wing model, ideal fuselage, propeller running;  $\epsilon_h = \text{body-fixed}$ ;  $\epsilon_l = 1.0$ ;  $\epsilon_q$  from  $-0.3$  to  $+0.3$ ).

Figure 65.- Mean additional angle of downwash due to slipstream (low-wing model, angular fuselage, propeller running;  $\epsilon_h = \text{body-fixed}$ ;  $\epsilon_l = 1.0$ ;  $\epsilon_q$  from  $-0.3$  to  $+0.3$ ).

Figure 66.- Apparent angle of downwash against  $\alpha$  (low-wing model with angular fuselage and propeller running;  $\epsilon_h = \text{body-fixed}$ ;  $\epsilon_l = 1.0$ ;  $\epsilon_q$  from  $-0.3$  to  $+0.3$ ).

Figure 67.- Stability coefficients (low-wing model; angular fuselage, propeller running;  $\epsilon_h = \text{body-fixed}$ ;  $\epsilon_l = 1.0$ ;  $\epsilon_q$  from  $-0.3$  to  $+0.3$ ).

Figure 68.- Stability coefficients (low-wing model; angular fuselage, propeller running;  $\epsilon_h = 0$  (wind-fixed);  $\epsilon_l = 1.0$ ;  $\epsilon_q$  from  $-0.3$  to  $+0.3$ ).

Figure 69.- Stability coefficients (low-wing model with ideal fuselage and propeller running;  $\epsilon_h = \text{body-fixed}$ ;  $\epsilon_l = 1.0$ ;  $\epsilon_q$  from  $-0.3$  to  $+0.3$ ).

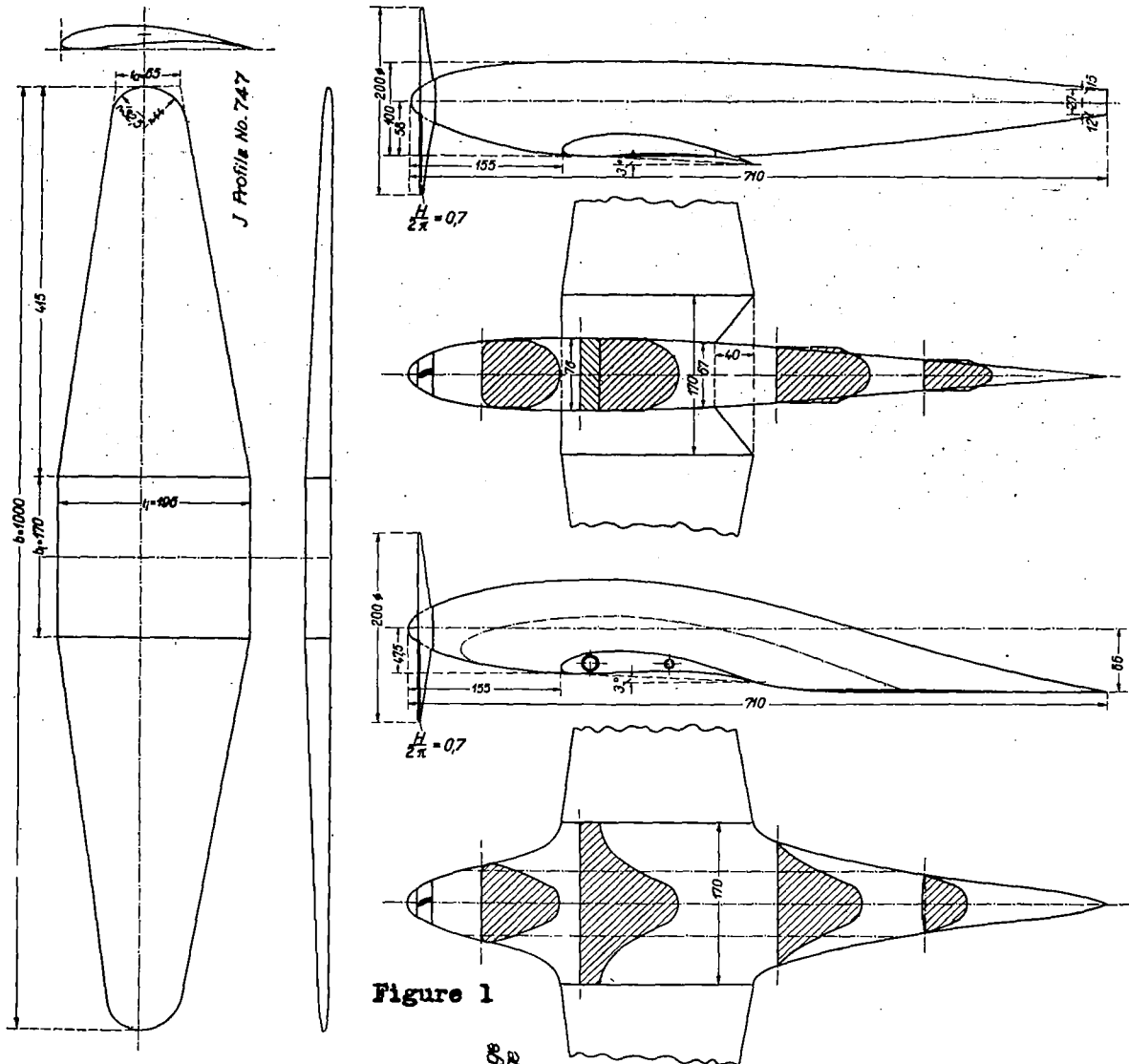


Figure 1

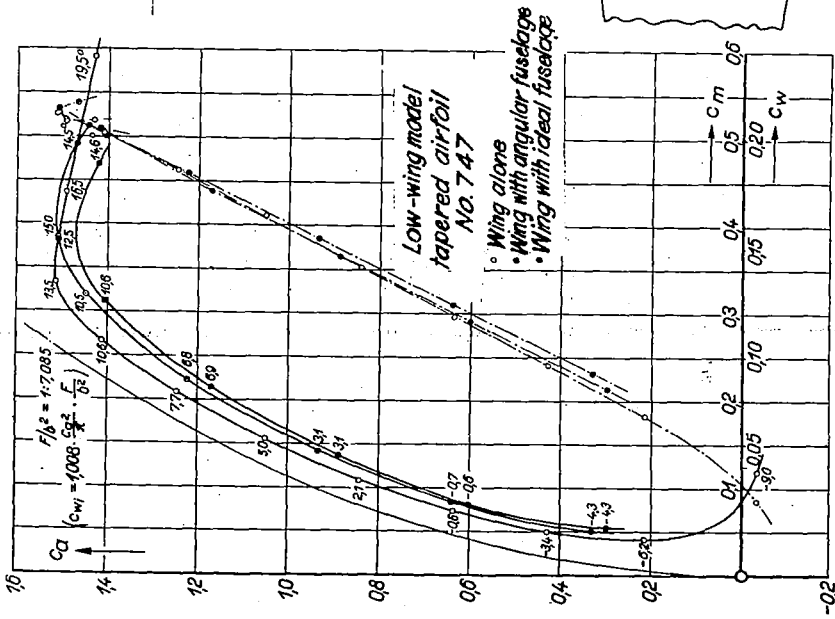


Figure 2

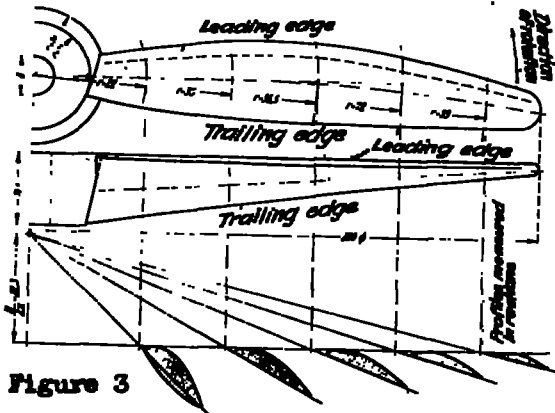


Figure 3

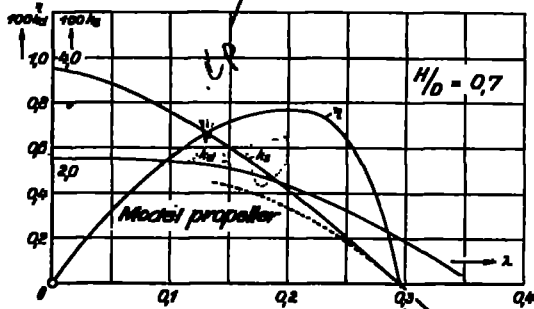


Figure 4

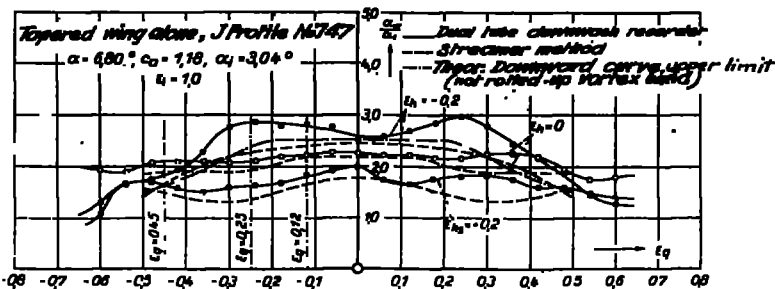


Figure 5

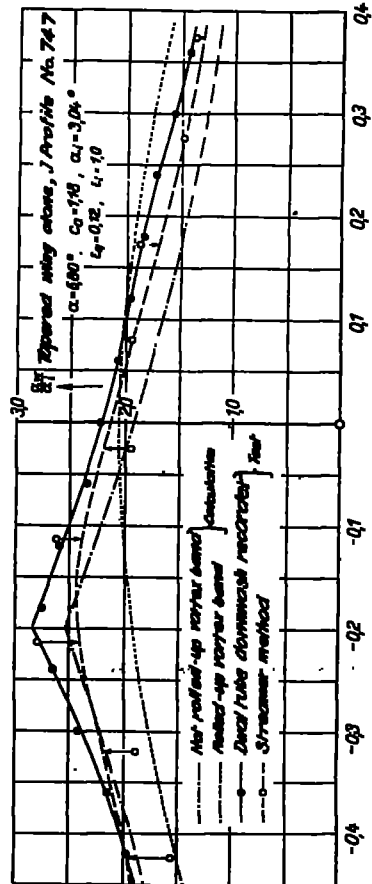


Figure 6

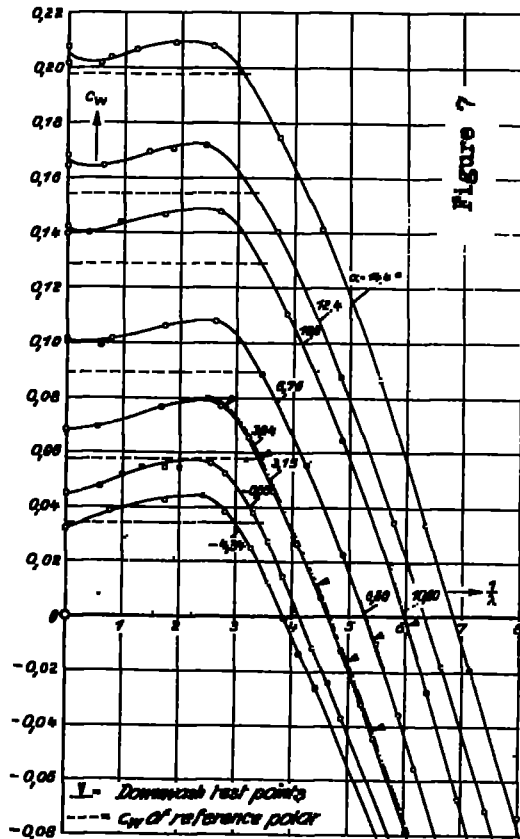


Figure 7

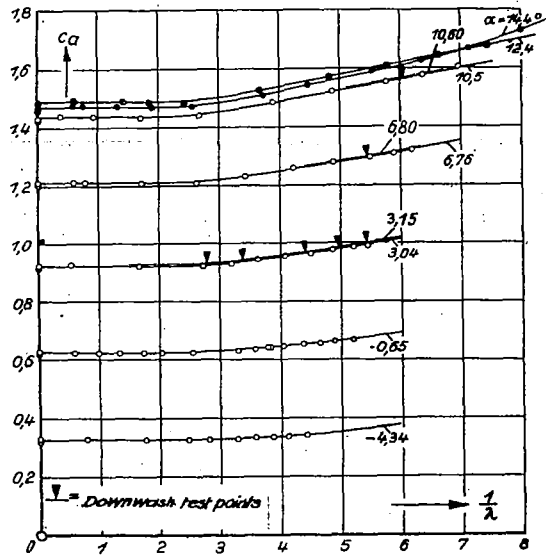


Figure 8

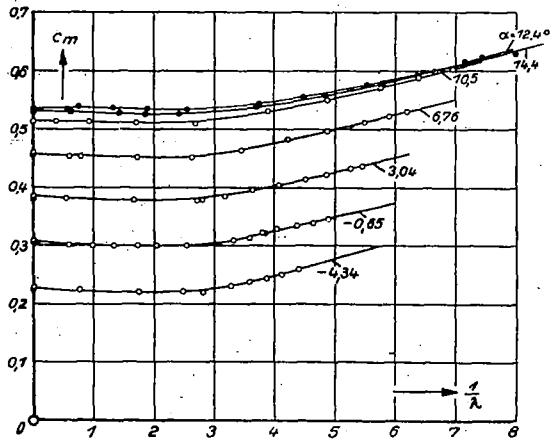


Figure 9

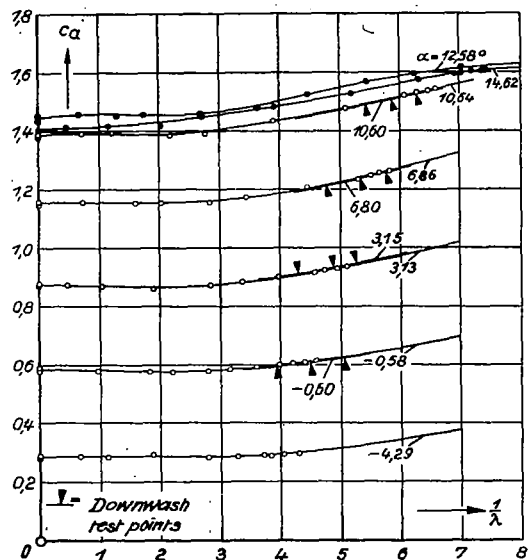


Figure 11

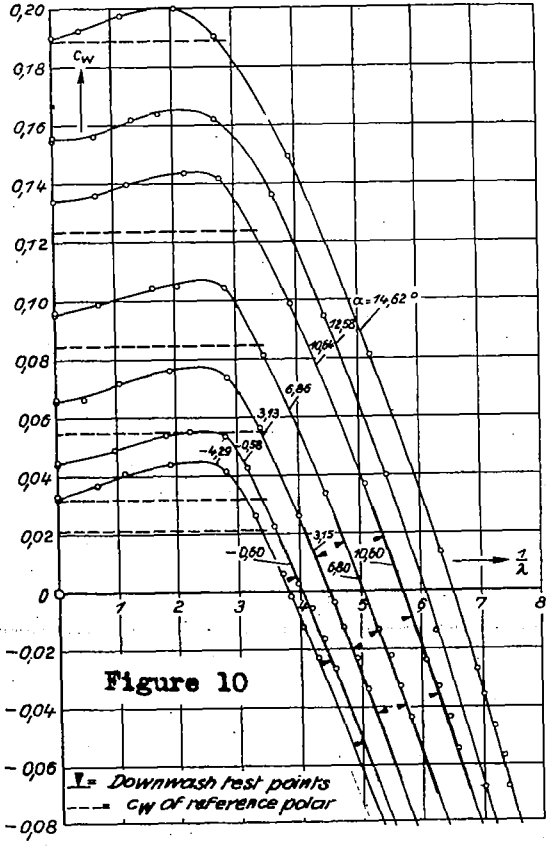


Figure 10

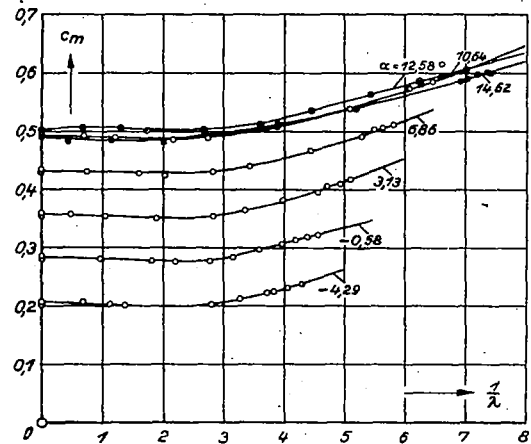


Figure 12

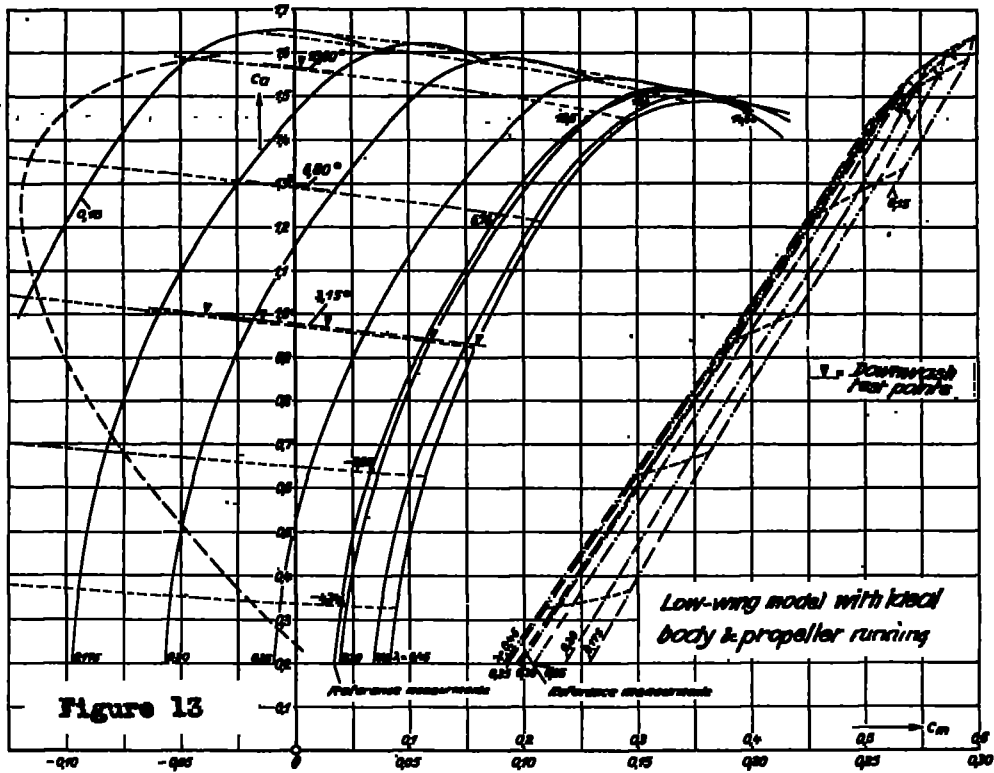


Figure 13

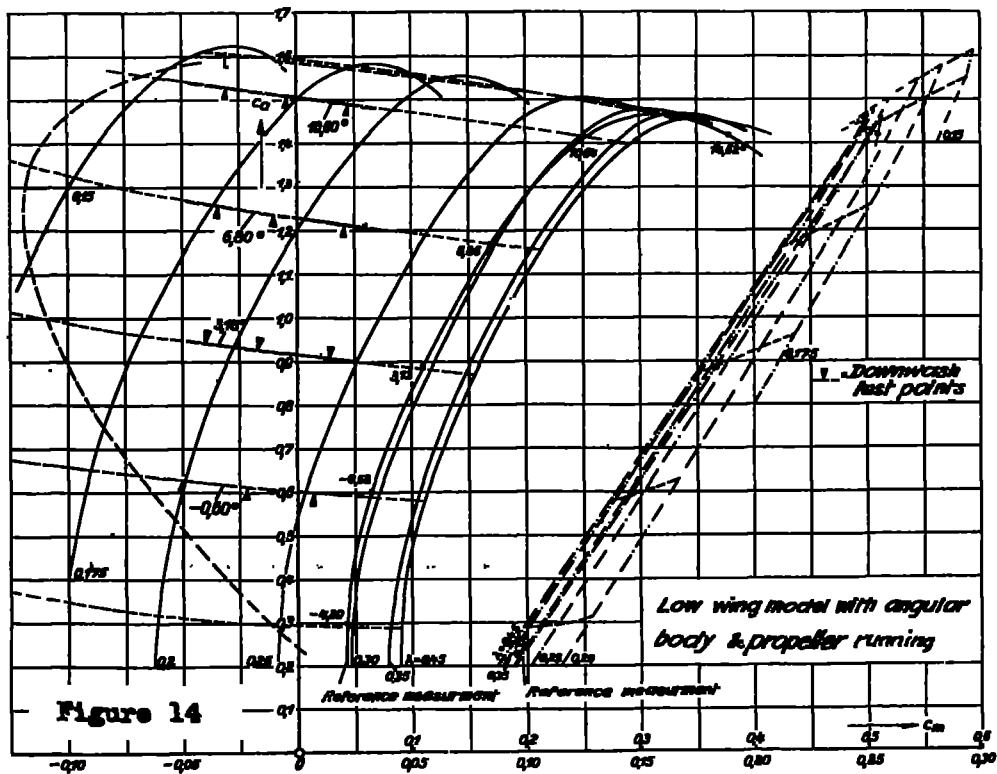


Figure 14

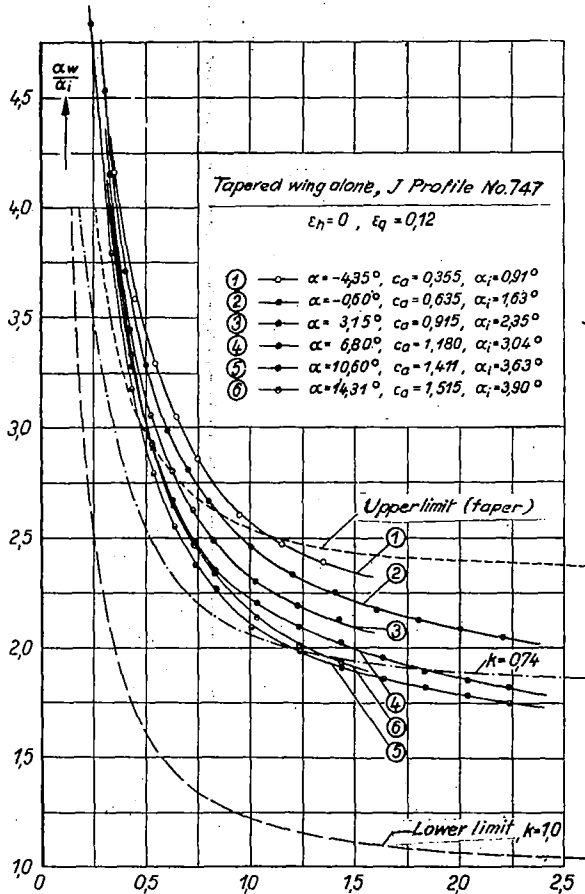


Figure 19

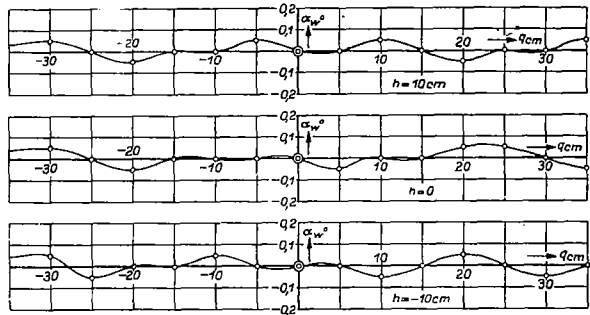


Figure 16

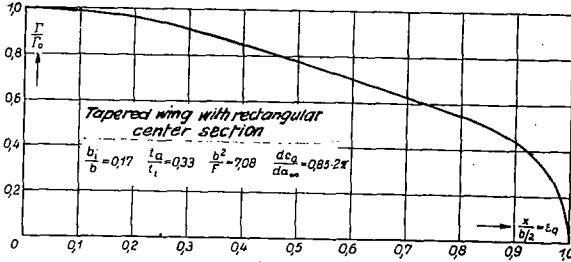


Figure 17

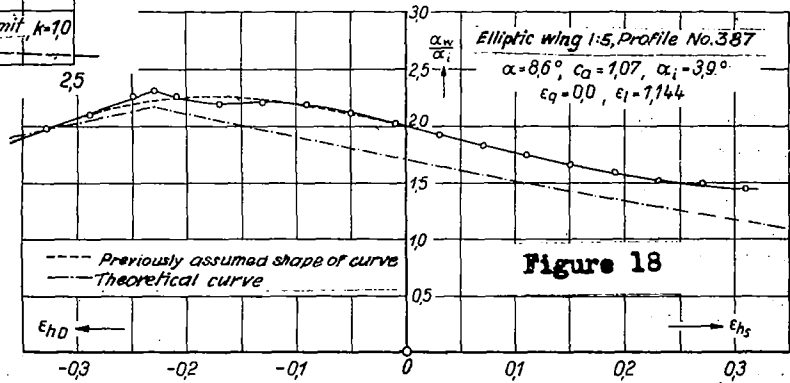


Figure 18

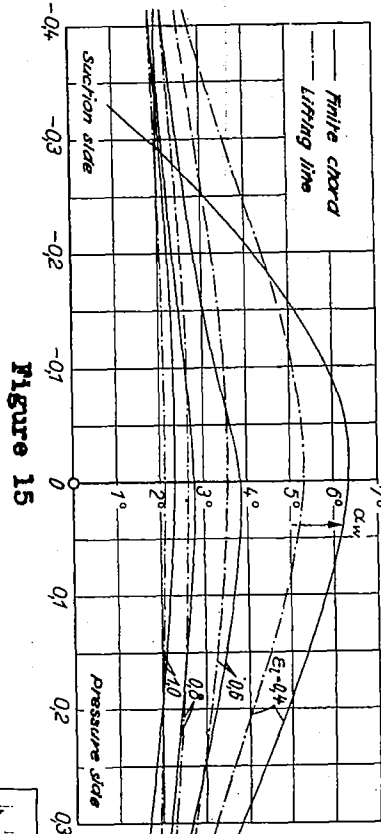


Figure 15

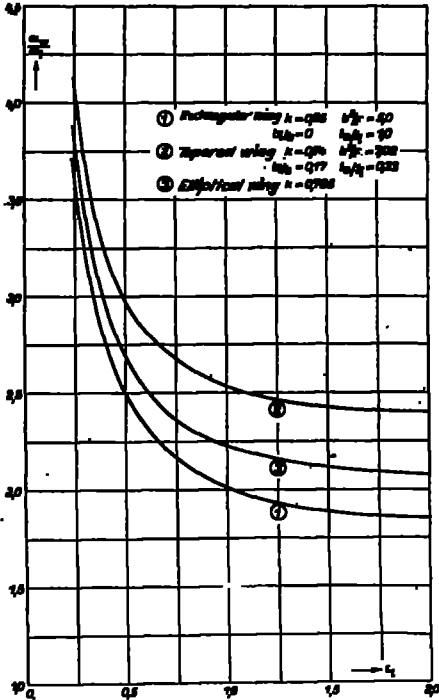


Figure 20

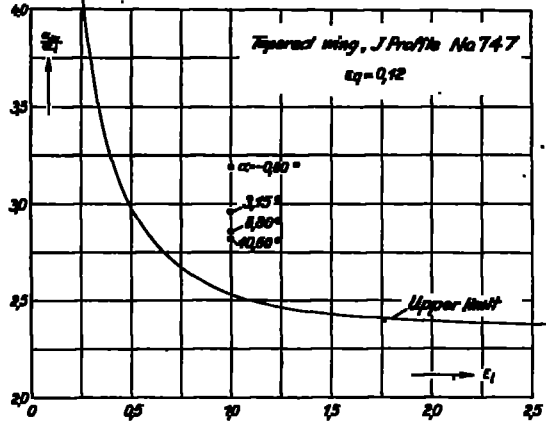


Figure 21

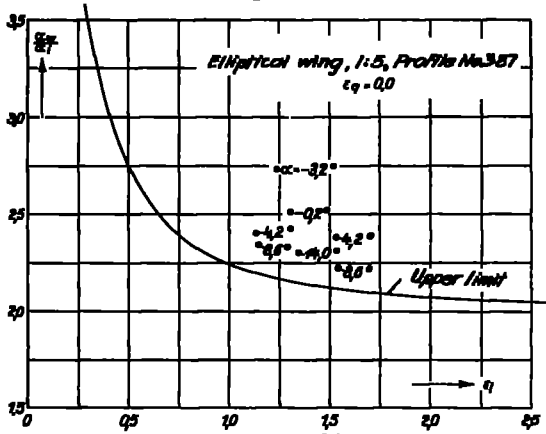


Figure 22

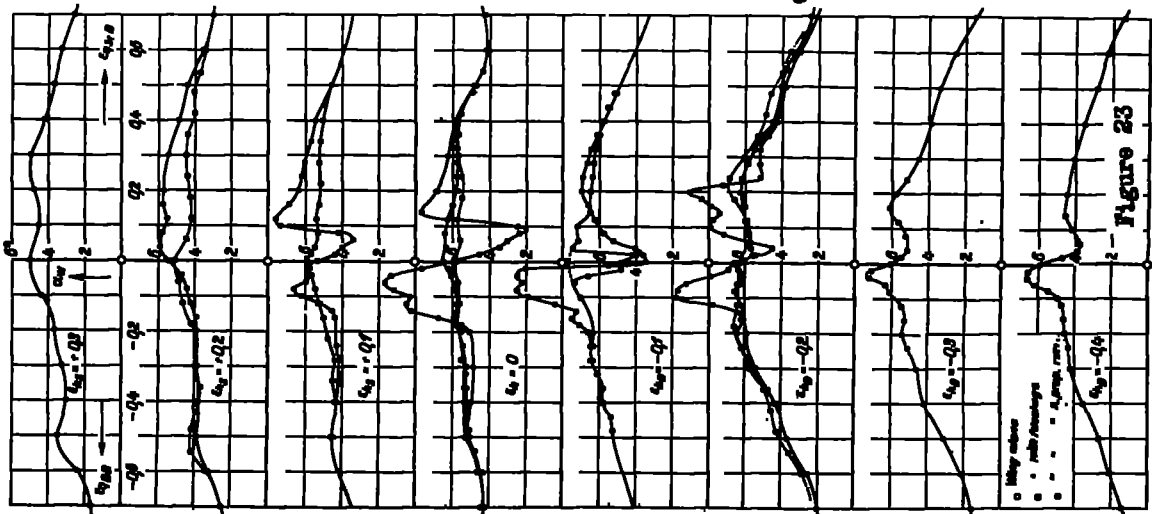


Figure 23

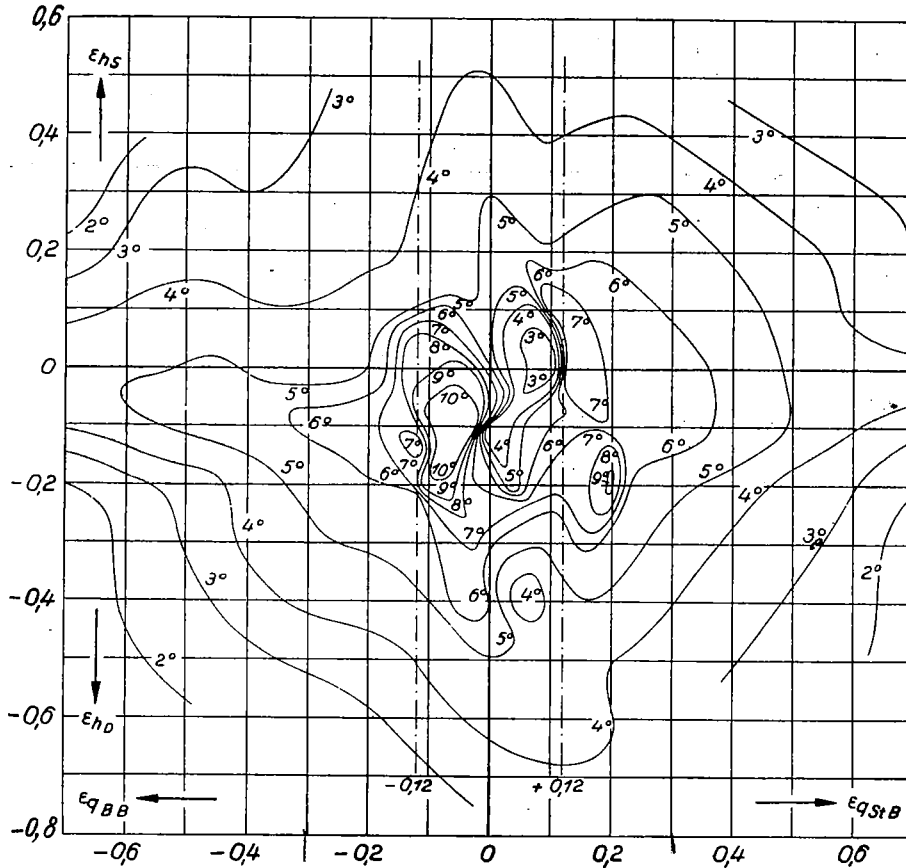


Figure 24

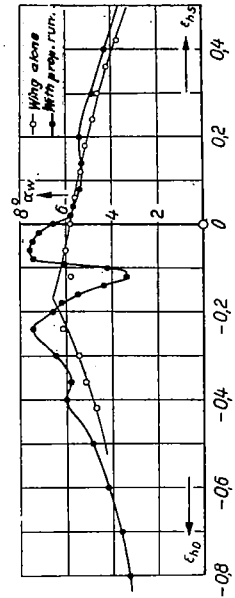


Figure 26

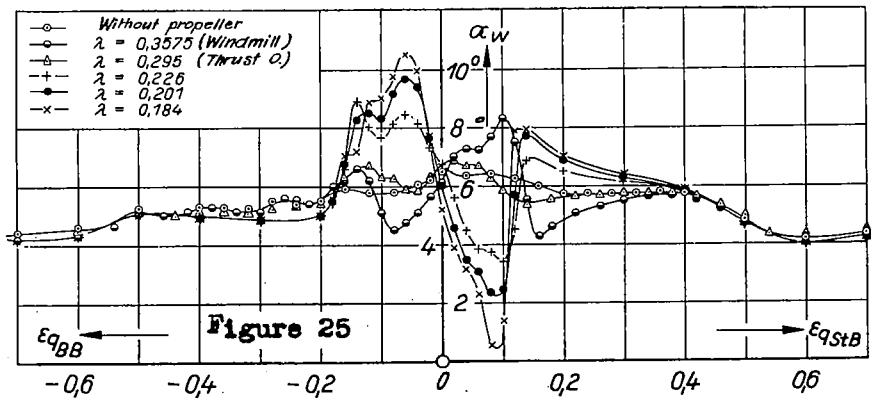


Figure 25

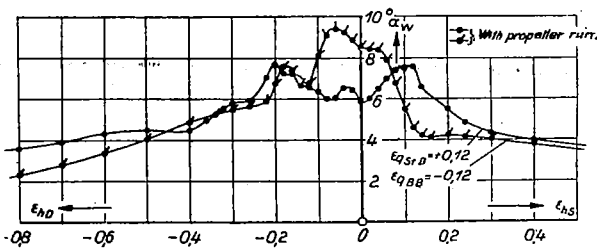


Figure 27

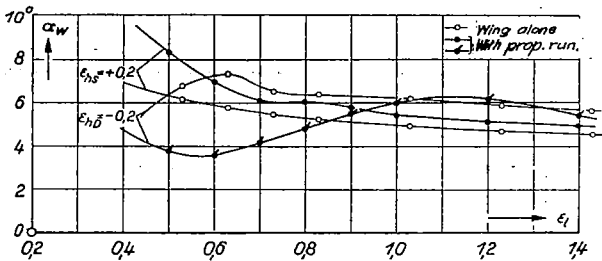


Figure 28

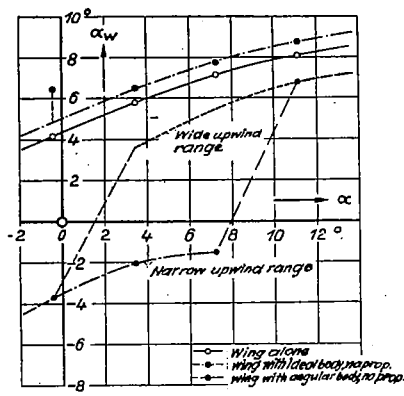
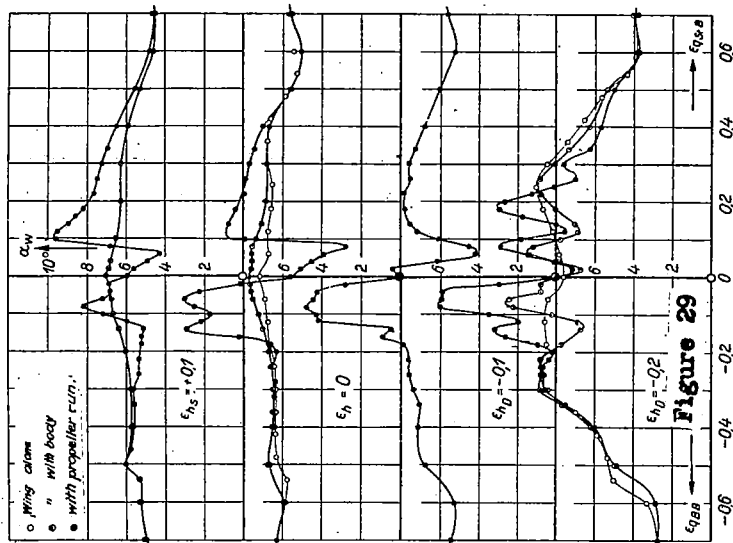


Figure 38

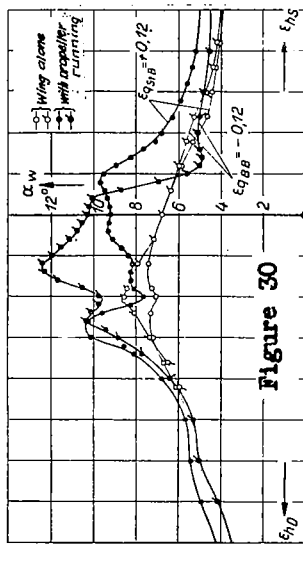


Figure 30

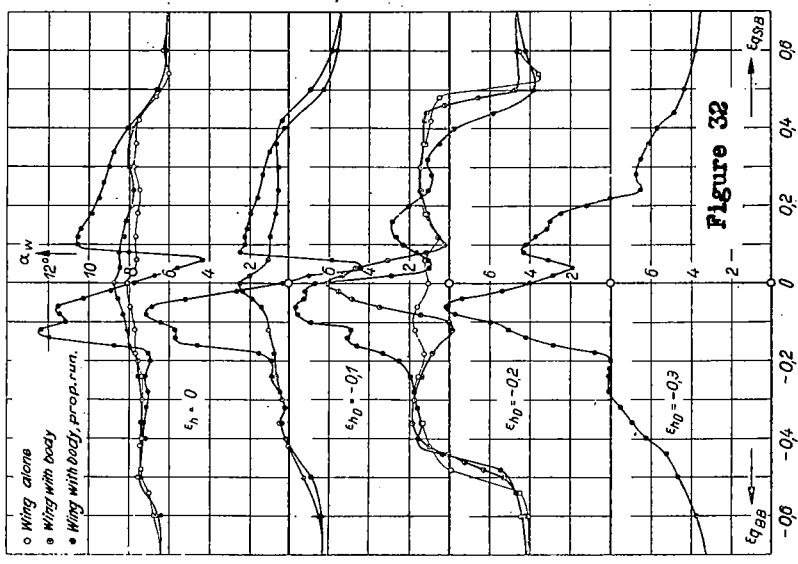


Figure 32

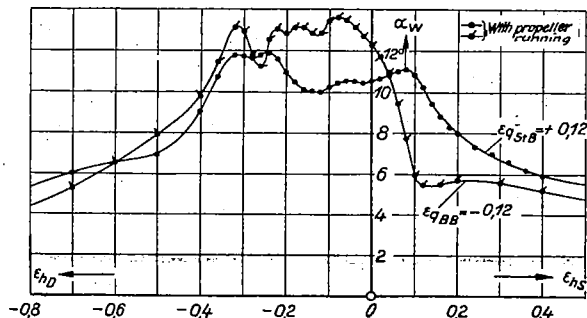


Figure 33

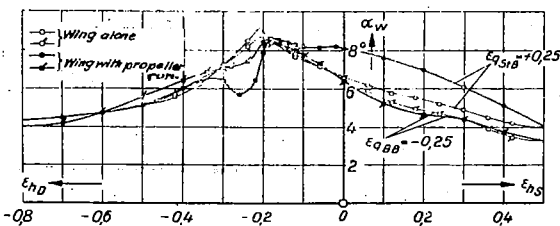


Figure 31

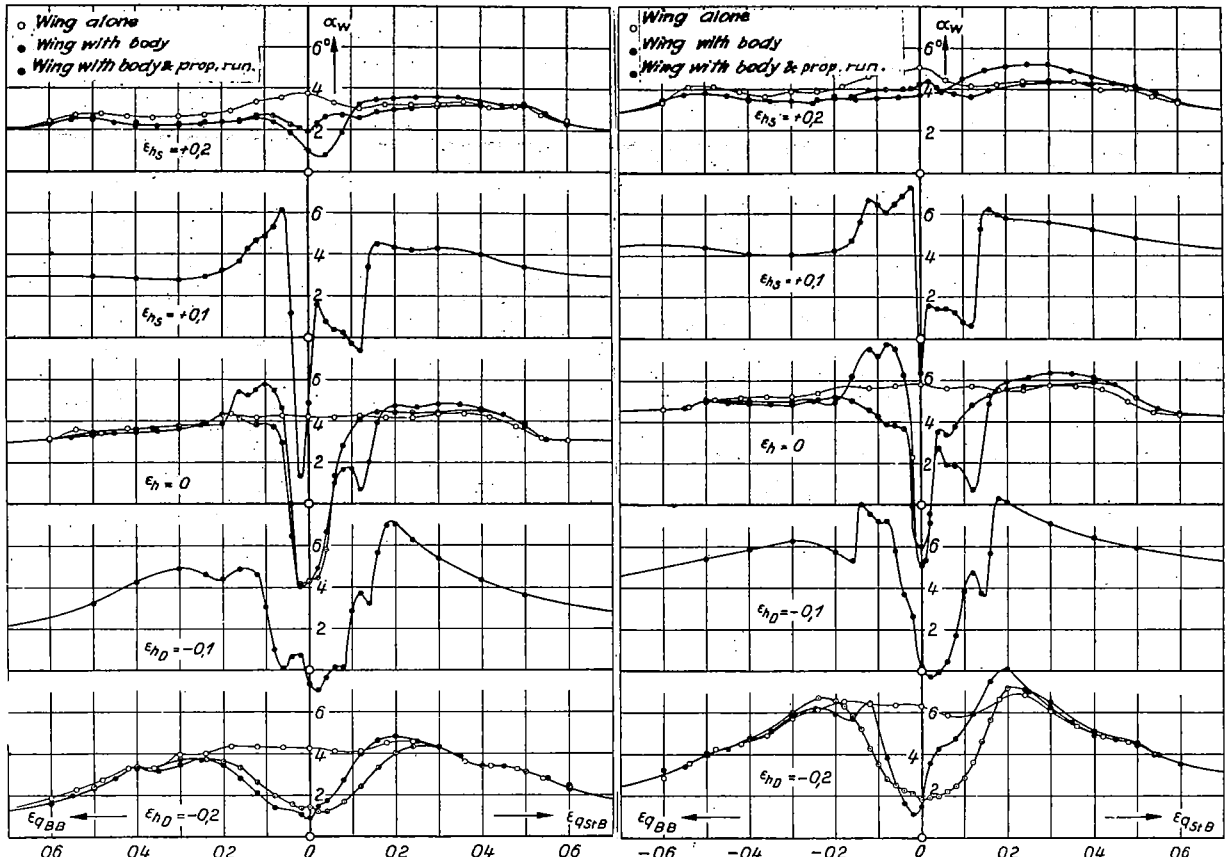


Figure 34

Figure 35

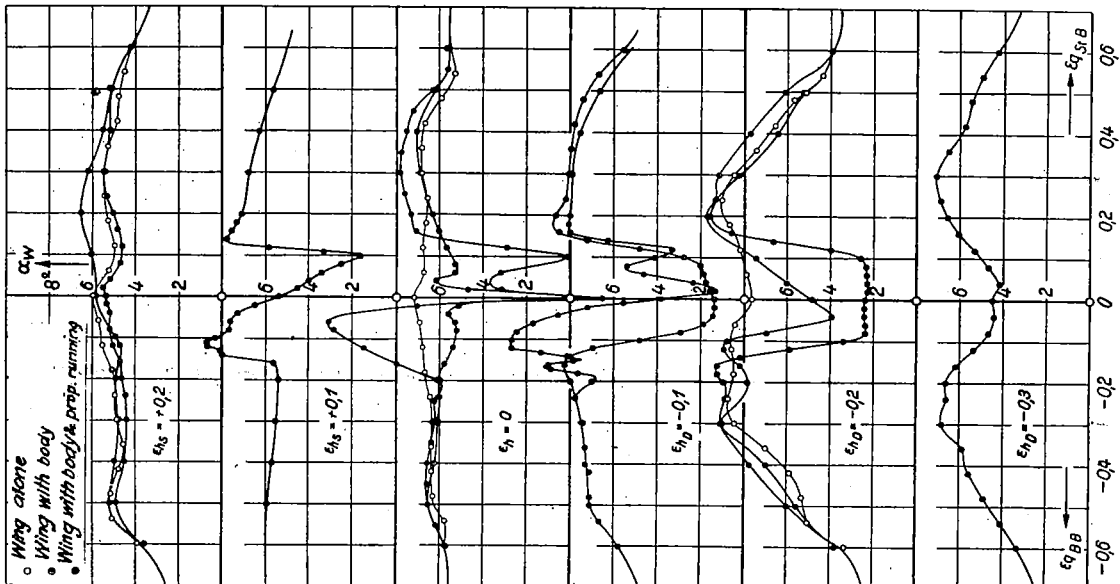


Figure 36

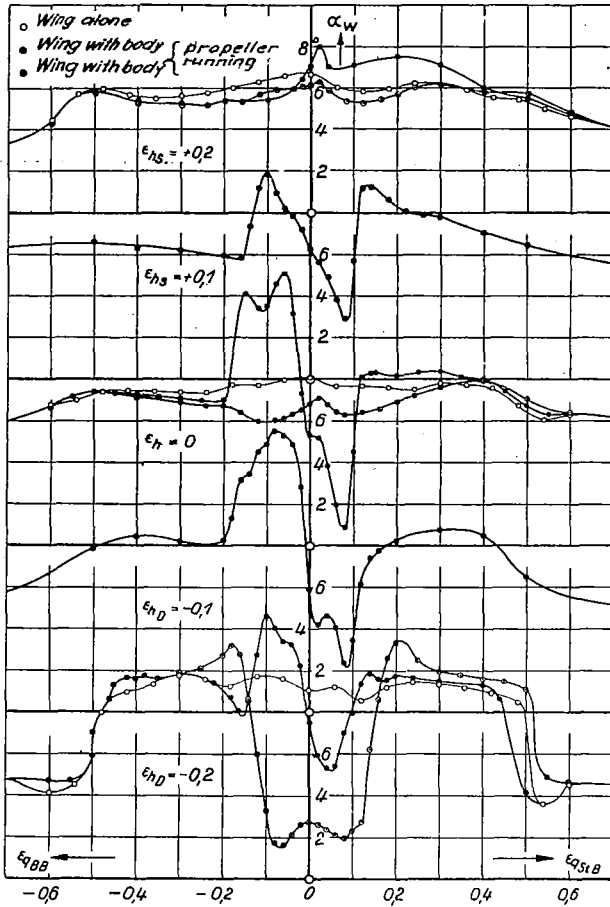


Figure 37

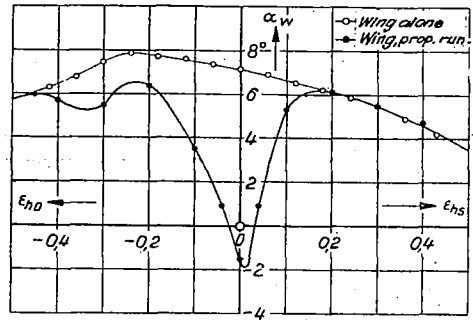


Figure 43

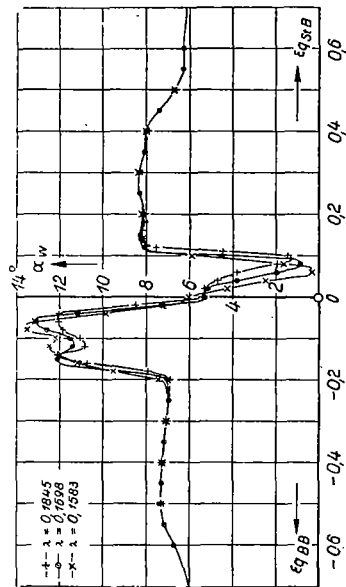


Figure 42

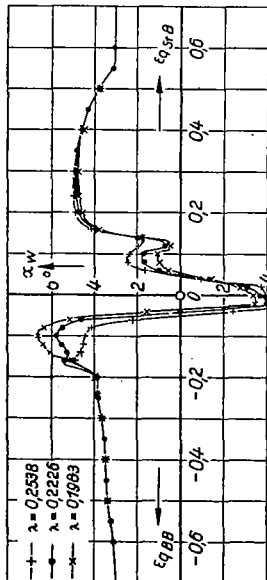


Figure 39

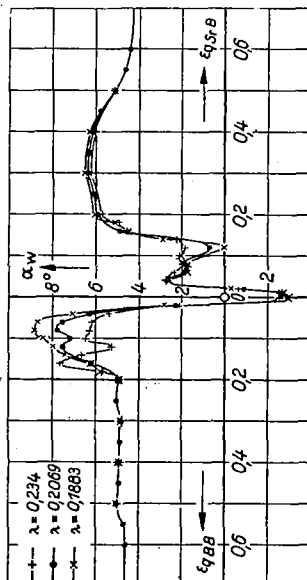


Figure 40

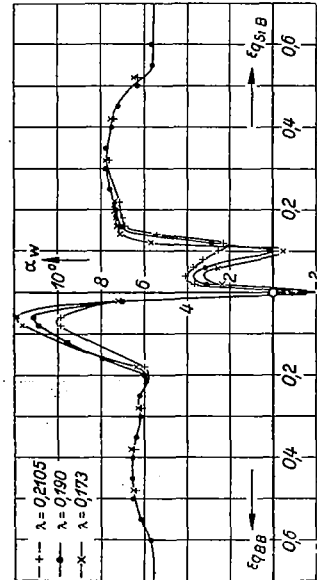


Figure 41

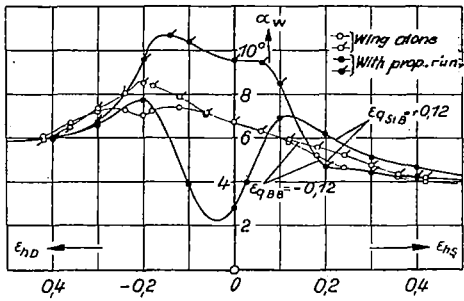


Figure 44

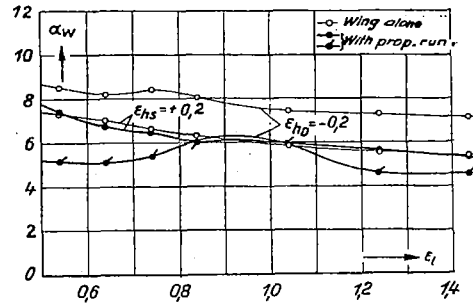


Figure 46

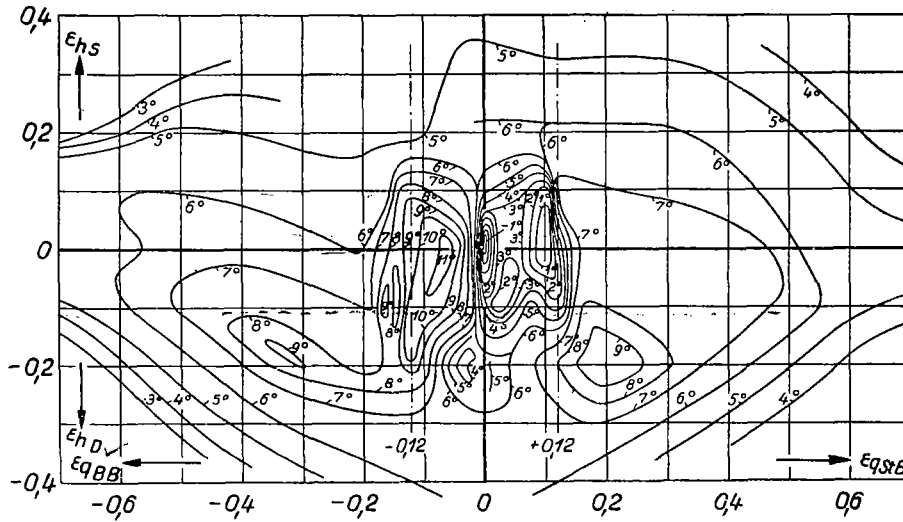


Figure 45

$A = 6.8$   
 $C_a = 1.18$   
 $d_p = 1.0$   
 $\lambda = 0.1885$

*Low wing  
 angular distance.*

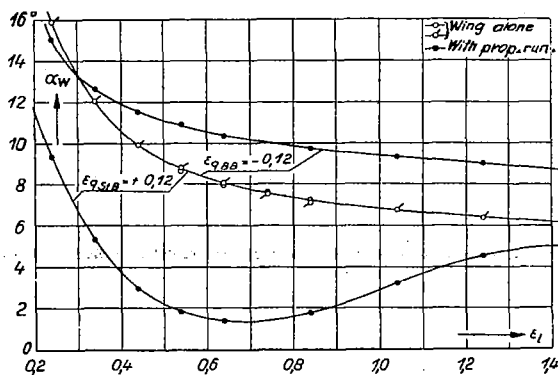


Figure 47

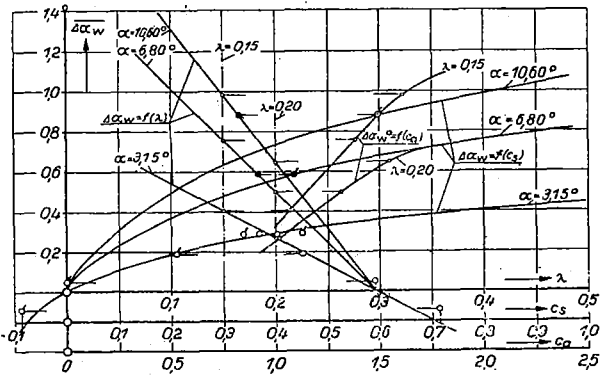


Figure 48

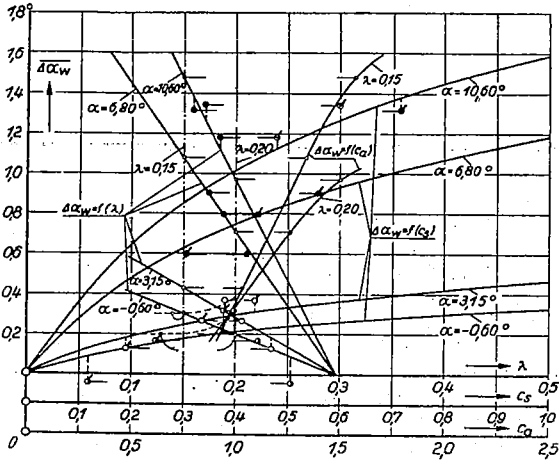


Figure 49

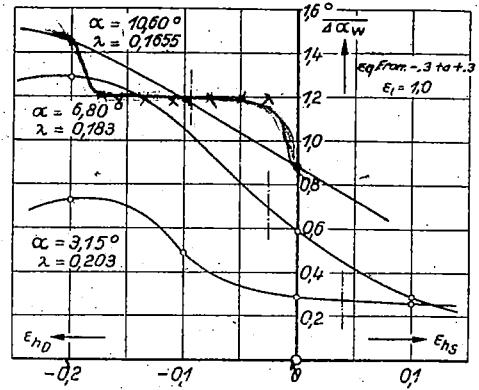


Figure 50

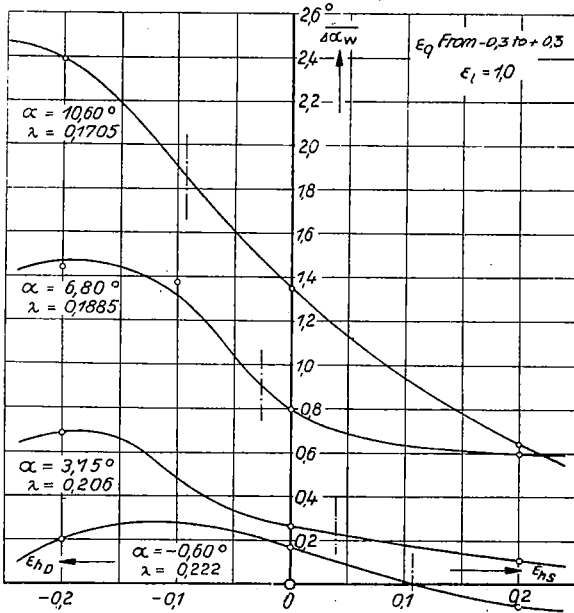


Figure 51

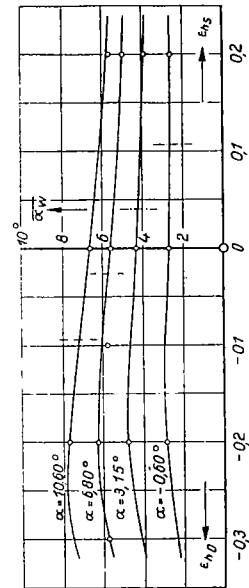


Figure 53

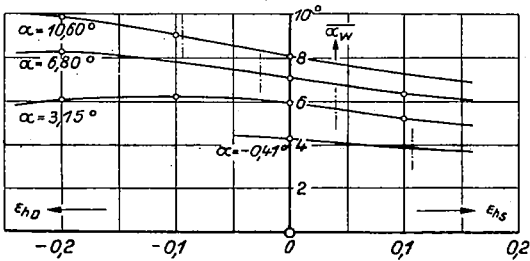


Figure 52

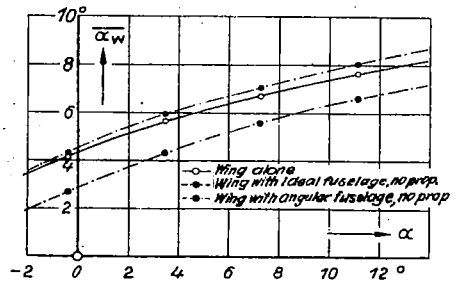


Figure 54

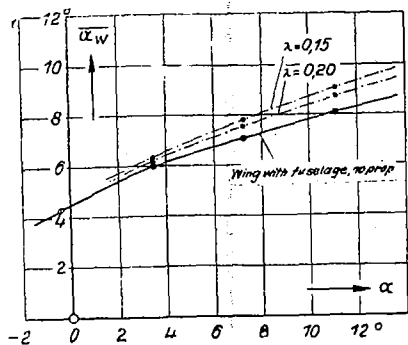


Figure 55

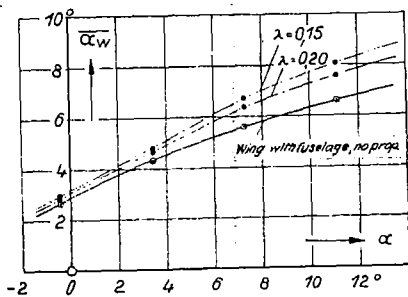


Figure 56

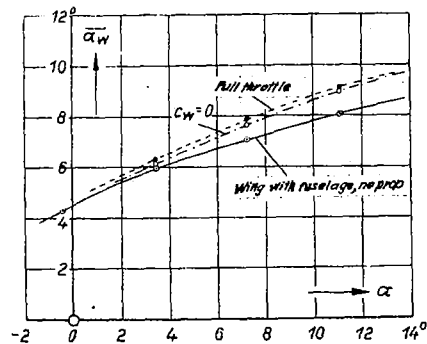


Figure 57

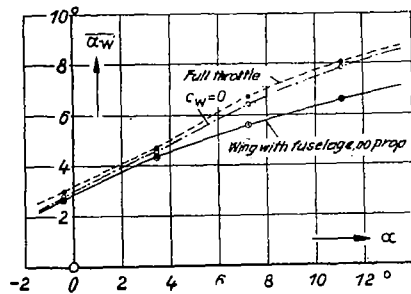


Figure 58

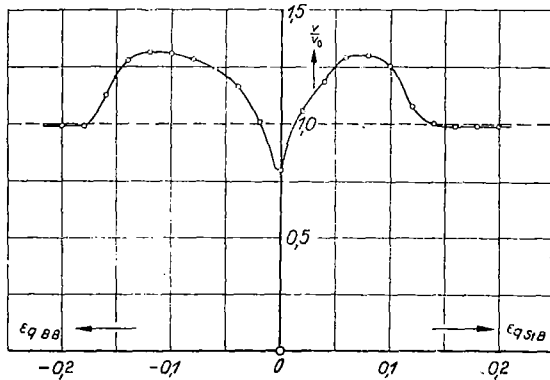


Figure 59

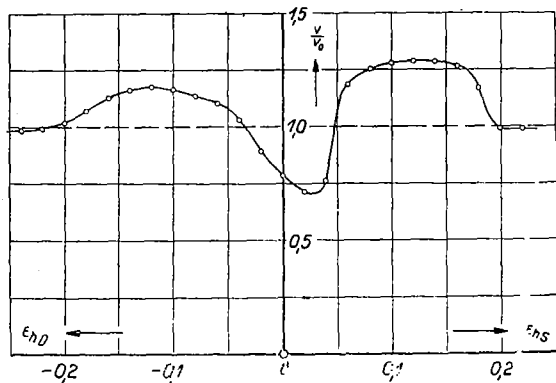


Figure 60

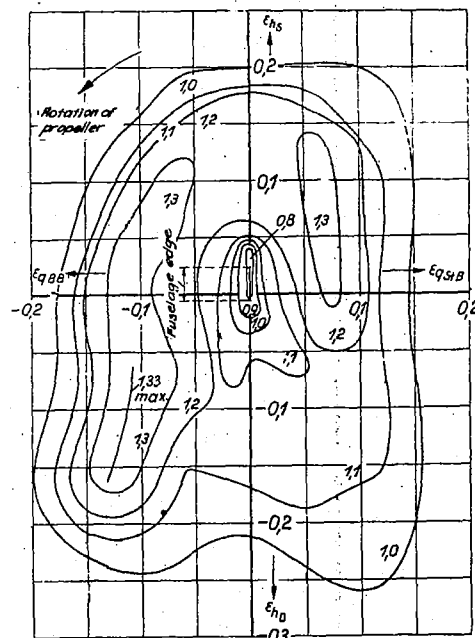


Figure 61

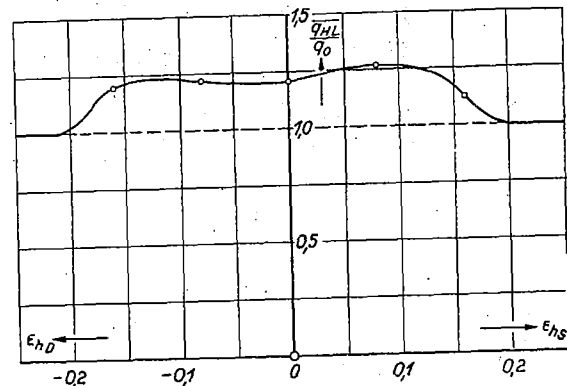
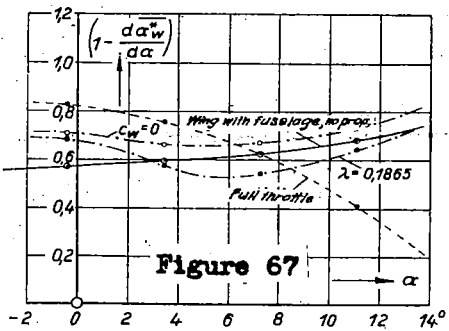
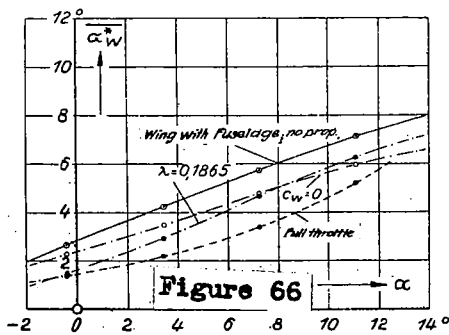
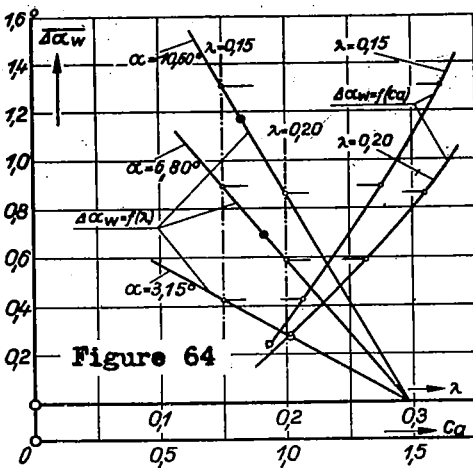
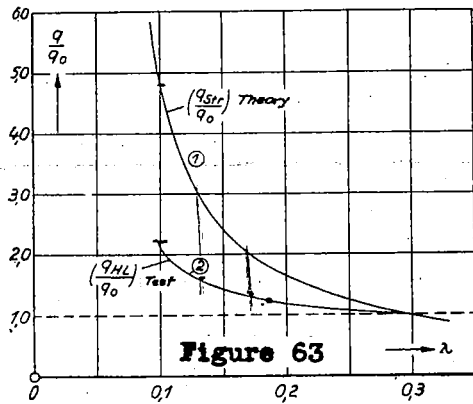
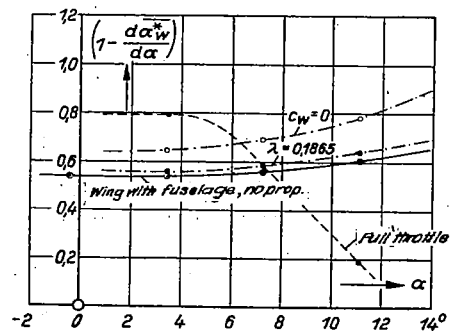
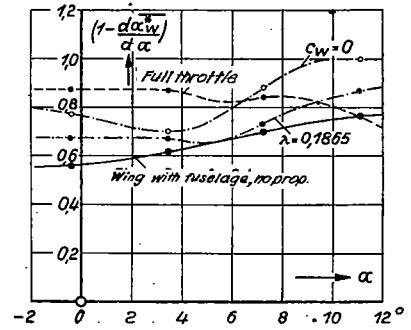
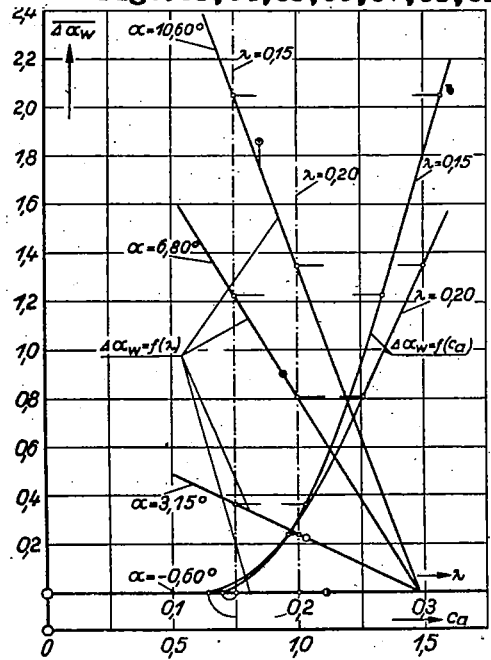


Figure 62



**Figs. 63, 64, 65, 66, 67, 68, 69**



NASA Technical Library



3 1176 01440 3563